This is a repository copy of *Biophysical and morphological changes in inner hair cells and their efferent innervation in the ageing mouse cochlea*.

Biophysical and morphological changes in inner hair cells and their efferent innervation in the ageing mouse cochlea

Jing-Yi Jeng[1], Adam J. Carlton[1] (iD), Stuart L. Johnson[1,2], Steve D. M. Brown[3], Matthew C. Holley[1] (iD), Michael R. Bowl[3] (iD) and Walter Marcotti[1,2] (iD)

[1] *Department of Biomedical Science, University of Sheffield, Sheffield, UK*
[2] *Neuroscience Institute, University of Sheffield, Sheffield, UK*
[3] *Mammalian Genetics Unit, MRC Harwell Institute, Oxfordshire, UK*

Edited by: Kim Barrett & Ian Forsythe

> **Key points**
>
> - Age-related hearing loss is a progressive hearing loss involving environmental and genetic factors, leading to a decrease in hearing sensitivity, threshold and speech discrimination.
> - We compared age-related changes in inner hair cells (IHCs) between four mouse strains with different levels of progressive hearing loss.
> - The surface area of apical coil IHCs (9–12 kHz cochlear region) decreases by about 30–40% with age.
> - The number of BK channels progressively decreases with age in the IHCs from most mouse strains, but the basolateral membrane current profile remains unchanged.
> - The mechanoelectrical transducer current is smaller in mice harbouring the hypo-morphic *Cdh23* allele *Cdh23*^{ahl} (C57BL/6J; C57BL/6NTac), but not in *Cdh23*-repaired mice (C57BL/6NTac^{Cdh23+}), indicating that it could contribute to the different progression of hearing loss among mouse strains.
> - The degree of efferent rewiring onto aged IHCs, most likely coming from the lateral olivocochlea fibres, was correlated with hearing loss in the different mouse strains.

Abstract   Inner hair cells (IHCs) are the primary sensory receptors of the mammalian cochlea, transducing acoustic information into electrical signals that are relayed to the afferent neurons. Functional changes in IHCs are a potential cause of age-related hearing loss. Here, we have investigated the functional characteristics of IHCs from early-onset hearing loss mice harbouring the allele *Cdh23*^{ahl} (C57BL/6J and C57BL/6NTac), from late-onset hearing loss mice (C3H/HeJ), and from mice corrected for the *Cdh23*^{ahl} mutation (C57BL/6NTac^{Cdh23+}) with an intermediate hearing phenotype. There was no significant loss of IHCs in the 9–12 kHz cochlear region up to at least 15 months of age, but their surface area decreased progressively by 30–40% starting from ∼6 months of age. Although the size of the BK current decreased with age, IHCs retained a normal KCNQ4 current and resting membrane potential. These basolateral membrane changes were most severe for C57BL/6J and C57BL/6NTac, less so for C57BL/6NTac^{Cdh23+} and minimal or absent in C3H/HeJ mice. We also found that lateral olivocochlear (LOC) efferent fibres re-form functional

Jing-Yi Jeng received her MSc degree in Biotechnology at National Tsing Hua University (Taiwan) and her PhD in Biomedical Science at the University of Sheffield (UK). Her research aims to understand the physiological mechanisms crucial for the development and ageing of the cochlear hair cells in the mammalian cochlea. She is a Postdoctoral Research Associate within the Hearing Research Group (https://www.sheffield.ac.uk/hearing) in the Department of Biomedical Science at the University of Sheffield (UK).
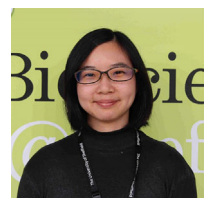
axon-somatic connections with aged IHCs, but this was seen only sporadically in C3H/HeJ mice. The efferent post-synaptic SK2 channels appear prior to the establishment of the efferent contacts, suggesting that IHCs may play a direct role in re-establishing the LOC-IHC synapses. Finally, we showed that the size of the mechanoelectrical transducer (MET) current from IHCs decreased significantly with age in mice harbouring the $Cdh23^{ahl}$ allele but not in C57BL/6NTac^{Cdh23+} mice, indicating that the MET apparatus directly contributes to the progression of age-related hearing loss.

Introduction

Age-related hearing loss (ARHL), also known as presbycusis, is a chronic disorder in which patients suffer from progressive loss of hearing sensitivity and the ability to understand speech with age. It is one of the most common forms of hearing loss in adults over 60 years old (Bowl & Dawson, 2019). Age-related hearing loss involves numerous risk factors ranging from genetics to lifestyle, with the underlying mechanisms remaining largely unknown. However, damage to the auditory receptors in the cochlea, namely the inner and outer hair cells (IHCs and OHCs) and their innervation, is likely to play a key role (Johnsson, 1974; Schuknecht & Gacek, 1993; Sergeyenko *et al.* 2013; Tawfik *et al.* 2019; Wu *et al.* 2019; Jimenez *et al.* 2020). Although we now have a better understanding of age-related changes in OHCs (Jeng *et al.* 2020a) and IHC ribbon synapses (Jeng *et al.* 2020b), very little is known about how the biophysical properties of IHCs and their efferent innervation are affected by cochlear ageing, which limits our understanding of how IHC function contributes to the progression of ARHL.

In the adult mammalian cochlea, sound-induced displacement of the hair cell stereociliary bundles regulates the gating of mechanoelectrical transducer (MET) channels located at the tips of the shorter rows of stereocilia (Beurg *et al.* 2009). The depolarizing MET current, which is mainly carried by K^+ but also by Ca^{2+} ions, generates a receptor potential that modulates the release of glutamate from IHC ribbon synapses onto the spiral ganglion afferent terminals (Marcotti, 2012; Johnson *et al.* 2019). IHC membrane repolarization is then achieved by the activation of two characteristic basolateral membrane K^+ channels, which carry the negatively activating K^+ current $I_{K,n}$, and the large-conductance Ca^{2+}-activated K^+ current $I_{K,f}$ (Marcotti *et al.* 2003; Oliver *et al.* 2003). In the absence of sound stimulation, these hyperpolarizing K^+ currents are 'balanced' by the depolarizing resting MET current in order to set the resting membrane potential of IHCs to near -60 mV (Johnson *et al.* 2011), which is just positive to the activation of the $Ca_V1.3$ Ca^{2+} channels in adult cells

(Zampini *et al.* 2013). Crucial to IHC function is their neuronal innervation pattern, with each IHC making exclusive contact (Pujol *et al.* 1998) with up to $\sim$20 type I spiral ganglion afferent fibres in mice (Meyer *et al.* 2009). In addition, the cochlear sensory epithelium is innervated by cholinergic lateral olivocochlear (LOC) efferent fibres, which descend from the brainstem and form axo-dendritic synapses with type I afferent terminals below the IHCs (Maison *et al.* 2003). However, recent studies have shown that in $\sim$1-year-old cochleae of C57BL/6J mice the efferent system undergoes major rewiring, with the reappearance of direct axo-somatic efferent synapses onto aged IHCs (Lauer *et al.* 2012; Zachary & Fuchs 2015) that are normally present only during the pre-hearing stages of development (Glowatzki & Fuchs 2000).

Here, we have used mice with early-onset (C57BL/6J and C57BL/6NTac) and late-onset hearing loss (C57BL/6NTac^{Cdh23+} and C3H/HeJ) to identify changes in the morphological and biophysical properties of IHCs and their efferent synapses with age and to consider which of those changes could influence the temporal progression of ARHL. C57BL/6J and C57BL/6NTac strains harbour a hypomorphic allele in *Cadherin 23* ($Cdh23^{ahl}$) (Johnson *et al.* 1997; Noben-Trauth *et al.* 2003; Mianné *et al.* 2016). *Cadherin 23* encodes cadherin-23 that, together with protocadherin-15, forms the tip links required for gating the MET channels (Kazmierczak *et al.* 2007). Correction of the $Cdh23^{ahl}$ allele, using CRISPR/Cas9 (C57BL/6NTac^{Cdh23+} mice), delays the onset hearing loss in the repaired mice (Mianné *et al.* 2016). Like CBA/CaJ, C3H/HeJ mice show a very slow decline in their hearing thresholds with age (Trune *et al.* 1996; Ohlemiller *et al.* 2016). We show that by 6 months of age all IHCs from the four mouse strains have a smaller surface area. The size of $I_{K,f}$, but not that of $I_{K,n}$, was reduced with age in most mouse strains. Despite these basolateral membrane changes, IHCs remained functional in older mice, as exemplified by normal auditory brainstem response (ABR) thresholds in the C3H strain (see also Jeng *et al.* 2020b). Efferent synapses underwent age-related morphological and physiological

changes that were correlated with hearing loss measured in the 12 kHz cochlear region of the different strains (6N and 6J > 6N-Repaired). C3H mice had normal hearing at 12–13 months of age and few or no measurable changes in their IHCs or associated efferent synapses. We also discovered that the MET current in aged IHCs was differentially affected between C57BL/6NTac and C57BL/6NTac^{Cdh23+} mice, suggesting that it may be involved in the progression of ARHL.

Materials and methods

Ethics statement

All animal work was performed at the University of Sheffield (UK), licensed by the Home Office under the Animals (Scientific Procedures) Act 1986 (PPL_PCC8E5E93) and approved by the University of Sheffield Ethical Review Committee (180626_Mar). Auditory brainstem responses in mice were performed following intraperitoneal injection of the anaesthetic solution: ketamine (100 mg kg^{-1} body weight, Fort Dodge Animal Health, Fort Dodge, IA, USA) and xylazine (10 mg kg^{-1}, Rompun 2%, Bayer HealthCare LLC, NY, USA). Mice were then either killed by a schedule 1 method (cervical dislocation) for *in vitro* experiments or recovered from anaesthesia with intraperitoneal injection of atipamezole (1 mg kg^{-1}). Mice under recovery from anaesthesia were returned to their cage, placed on a thermal mat and monitored over the following 2 to 4 h. Once able to move well and to respond to external stimuli they were returned to their holding racks.

Auditory brainstem responses

Auditory brainstem responses were recorded from male and female mice at 12–14 months of age in a soundproof chamber (MAC-3 Acoustic Chamber, IAC Acoustic, UK) as previously described (Ingham *et al.* 2011). Briefly, stimuli were delivered to the ear by calibrated loudspeakers (MF1-S, Multi Field Speaker, Tucker-Davis Technologies, FL, USA) placed 10 cm from the animal's pinna. Sound pressure was calibrated with a low-noise microphone probe system (ER10B+, Etymotic, IL, USA). Experiments were performed using customized software (Ingham *et al.* 2011) driving an RZ6 auditory processor (Tucker-Davis Technologies). Response thresholds were estimated from the resulting ABR waveform and defined as the lowest sound level at which any recognisable feature of the waveform was visible. Auditory brainstem response thresholds were independently evaluated by at least three members of the laboratory without prior knowledge of the mouse strain or sex. Responses were measured for clicks and pure tones of frequencies at 6, 12, 18, 24, 30, 36 and 42 kHz. Stimulus sound pressure levels were typically 0–95 dB SPL, presented in steps of 5 dB SPL. The brainstem response signals were averaged over 256 repetitions. Tone bursts were 5 ms in duration with a 1 ms on/off ramp time, which was presented at a rate of 42.6/s.

Tissue preparation

Experiments were performed using acutely dissected organs of Corti obtained from 1- to 17-month-old mice of the strains C57BL/6N, C57BL/6J, C57BL/6NTac^{Cdh23+} and C3H/HeJ from both sexes. Organs of Corti were dissected using an extracellular solution containing (in mM): 135 NaCl, 5.8 KCl, 1.3 CaCl$_2$, 0.9 MgCl$_2$, 0.7 NaH$_2$PO$_4$, 5.6 D-glucose, 10 Hepes-NaOH. Sodium pyruvate (2 mM), amino acids and vitamins were added from concentrates (Thermo Fisher Scientific, UK). The pH was adjusted to 7.48 ($\sim$308 mmol kg^{-1}). The dissection procedure of the ageing mouse cochlea has been described previously (Jeng *et al.* 2020a). After dissection the isolated organ of Corti was transferred to a microscope chamber, immobilized with a nylon mesh fixed to a stainless steel ring and viewed using an upright microscope (Olympus BX51, Japan; Leica, DMLFS, Germany; Nikon FN-1, Japan). The microscope chamber was continuously perfused with extracellular solution by a peristaltic pump (Cole-Palmer, UK). Hair cells were observed with Nomarski Differential Interference Contrast optics ($\times$63 or $\times$60 water immersion objectives) and $\times$15 eyepieces.

Single-cell electrophysiology

For whole-cell basolateral K$^+$ current recordings from adult IHCs, experiments were performed as previously described (Corns *et al.* 2018; Jeng *et al.* 2020c) from apical coil IHCs positioned within the frequency range of $\sim$9–12 kHz (Müller *et al.* 2005). The patch pipette intracellular solution contained (in mM): 131 KCl, 3 MgCl$_2$, 1 EGTA-KOH, 5 Na$_2$ATP, 5 Hepes-KOH, 10 Na-phosphocreatine (pH was adjusted with 1M KOH to 7.28; 294 mmol kg^{-1}). Membrane currents and voltage responses were recorded at room temperature (20–24°C) with an Optopatch amplifier (Cairn Research Ltd, UK). Data acquisition was controlled by pClamp software using Digidata 1440A or 1550 boards (Molecular Devices, CA, USA). Recordings were low-pass filtered at 2.5 kHz (8-pole Bessel), sampled at 5 kHz and stored on a computer for off-line analysis (Origin: OriginLab, MA, USA). Membrane potentials in whole-cell recordings were corrected for the residual series resistance R_s after compensation (usually 70–90%) and the liquid junction potential of -4 mV measured between electrode and bath solutions. The different extracellular solutions containing acetylcholine chloride (ACh: A6625, Sigma-Aldrich, UK), elevated K$^+$ and a Ca^{2+}-free solution were applied by a

gravity-fed multichannel pipette positioned close to the patched hair cell.

Mechanoelectrical transducer currents were recorded in young adult and aged IHCs using a fluid jet from a pipette driven by a 25 mm diameter piezoelectric disc (Corns *et al.* 2014, 2018). These recordings were technically challenging and they have only been performed in a few IHCs. The fluid jet pipette tip had a diameter of 8–10 μm and was positioned near the hair bundles to elicit a maximal MET current. Mechanical stimuli were applied as 50 Hz sinusoids.

Immunofluorescence microscopy

Dissected inner ears from the above mouse strains were fixed with 4% paraformaldehyde in phosphate-buffered saline (PBS, pH 7.4) for 20 min at room temperature. The organs of Corti were dissected, rinsed three times for 10 min in PBS and incubated for 1 h at room temperature in PBS supplemented with 5% normal goat or horse serum and 0.5% Triton X-100. The samples were then incubated overnight at 37°C with the primary antibody in PBS supplemented with 1% of the specific serum. Primary antibodies were: mouse anti-myosin 7a (1:1000, Developmental Studies Hybridoma Bank, #138-1C), rabbit anti-myosin 7a (1:200, Proteus Biosciences, #25-6790), rabbit anti-SK2 (1:500, Sigma-Aldrich, P0483), goat anti-choline acetyltransferase (ChAT, 1:500, Millipore, AB144P) and mouse anti-ATP1A3 (Na$^+$/K$^+$ ATPase 3, 1:500, ThermoFisher, MA391). All primary antibodies were labelled with species-appropriate Alexa Fluor secondary antibodies for 1 h at 37°C, and then washed three times (10 min) in PBS. Samples were then rinsed a final time in PBS (10 min) and mounted in VECTASHIELD (H-1000, Vector Laboratories). The z-stack images were captured with either a Nikon A1 confocal microscope (Nikon CFI Plan Apo 60X Oil objective) or a Zeiss LSM 880 with AiryScan for super-resolution confocal microscopy from the Wolfson Light Microscope Facility at the University of Sheffield. Image stacks were processed with Fiji ImageJ analysis software. The number of SK2 puncta was counted by two members of the laboratory, without prior knowledge of the mouse strain and age, using the z-stack images of the immunolabelled proteins. Individual puncta were assigned to two separate groups (pillar or modiolar) defined by the centre of Myo7a immunolabelling near the basal membrane.

Statistical analysis

Statistical comparisons of means were made by Student's two-tailed *t* test or, for multiple comparisons, analysis of variance (one-way or two-way ANOVA followed by a suitable *post hoc* test) using GraphPad 8.3. For some comparisons we have also used Chi-square and Brown–Forsythe tests. For tone burst ABR stimulus data, due to the presence of values outside the threshold limit of our equipment (95 dB), we used the non-parametric Kruskal–Wallis statistical test, followed by Dunn's *post hoc* test. $P < 0.05$ was selected as the criterion for statistical significance. Only mean values with a similar variance between groups were compared. Mean values are quoted in text and figures as means $\pm$ SD.

Results

The four different mouse strains were selected to allow comparison of the pathophysiological differences between those with early-onset (C57BL/6J: 6J, C57BL/6NTac: 6N, Hequembourg & Liberman, 2001; Kane *et al.* 2012), isogenic C57BL/6NTac mice with the *Cdh23^{ahl}* allele mutation corrected with CRISPR/Cas9 (C57BL/6NTac^{Cdh23+}: 6N-Repaired, Mianné *et al.* 2016) and late-onset hearing loss (C3H/HeJ: C3H, Trune *et al.* 1996).

ABR thresholds in 1-year-old mice

Age-related hearing loss has been shown to vary not only among different inbred mouse strains, but also between males and females. Late-onset hearing loss mice, such as CBA mice, appear to exhibit sex-related differences in hearing sensitivity only later in life ($\sim$2 years of age: Guimaraes *et al.* 2004; Kobrina & Dent, 2019). However, hearing threshold differences between males and females have also been reported within the first year of life in both CBA and C57BL/6J mice, being much more pronounced in the latter strain (Henry, 2004). Therefore, hearing in male and female C3H, 6N-Repaired, 6N and 6J mice, kept under the same environmental conditions, was investigated by measuring ABRs, which measure the activity of the afferent auditory pathway downstream of the IHCs. Strain-matched aged females (Fig. 1*A*, 12–13 months) and males (Fig. 1*B*, 12–13 months) showed no significant difference in their ABR thresholds for clicks ($P = 0.3139$, two-way ANOVA). When the data from strain-matched females and males were combined (Fig. 1*C*), we found that click ABR thresholds were significantly elevated in both 6N and 6J mice compared with either C3H ($P = 0.0056$ and $P < 0.0001$, respectively, Tukey's *post hoc* test, one-way ANOVA) or 6N-Repaired mice ($P = 0.0158$ and $P < 0.0001$, respectively). There was no significant difference between the 6N-Repaired and C3H mice ($P = 0.9962$). The variance of the pure-tone ABR thresholds was significantly different among the different mouse strains (Fig. 1*D–G*: $P < 0.0001$ for both 12 kHz and 18 kHz, Brown–Forsythe test). We analysed

the 12 kHz frequency data in more detail as this region is within the range used for the *in vitro* experiments (see below). We found no significant difference in ABR thresholds at 12 kHz between males and females across the four strains ($P = 0.2654$, two-way ANOVA). At 12 kHz, the ABR thresholds for combined males and females was significantly different among strains ($P < 0.0001$, Kruskal–Wallis test), with the highest thresholds recorded from 6N and 6J mice, lower thresholds from 6N-Repaired and the lowest from C3H (for Dunn's *post hoc* test see Fig. 1 legend). This strain-specific difference in hearing thresholds at 12 kHz was also seen in older male mice (up to 18 months of age: Jeng *et al.* 2020b). We then sought to identify age-related changes in the biophysical and morphological characteristics of cochlear IHCs that are associated with the onset of hearing loss.

The size, but not the number, of IHCs was reduced with age

In vitro experiments were performed in the apical coil of the cochlea, which corresponds to the 9–12 kHz frequency range (Müller *et al.* 2005; see also Ceriani *et al.* 2019), in male and female mice. This region was selected because it is most easily accessible for reliable, single-cell electrophysiological recordings. Initially, we determined the number of IHCs in the ageing cochlea using the hair cell marker myosin 7a (Fig. 2*A* and *B*). We found that the number of IHCs in C3H mice measured at the four ages (1, 6, 12 and 15 months) was significantly higher compared with the other three strains ($P < 0.0001$ for all interactions, two-way ANOVA, Tukey's *post hoc* test, Fig. 2*C*). The number of IHCs was not significantly different between 6N-Repaired mice and either of the early-onset hearing loss mice (with 6N: $P = 0.9447$; with 6J, $P = 0.9645$). In addition, there was no difference between 6N and 6J strains ($P = 0.7453$). Within each strain, the number of IHCs decreased significantly between 1 and 15 months of age only in the 6J mice (Fig. 2*C*). These results indicate that the loss of IHCs in the 9–12 kHz cochlea region is minimal or absent, at least up to 15 months of age in all strains. However, C3H mice have about 20% more IHCs than the other strains throughout life (Fig. 2*C*).

Although the number of IHCs remained relatively constant with age, the cells appeared to become smaller at older ages (Fig. 2*A* and *B*). We quantified the sizes of IHCs by measuring the total membrane capacitance (C_m) with the built-in circuitry of the Optopatch amplifier, which provides an electrical estimate of the cell surface
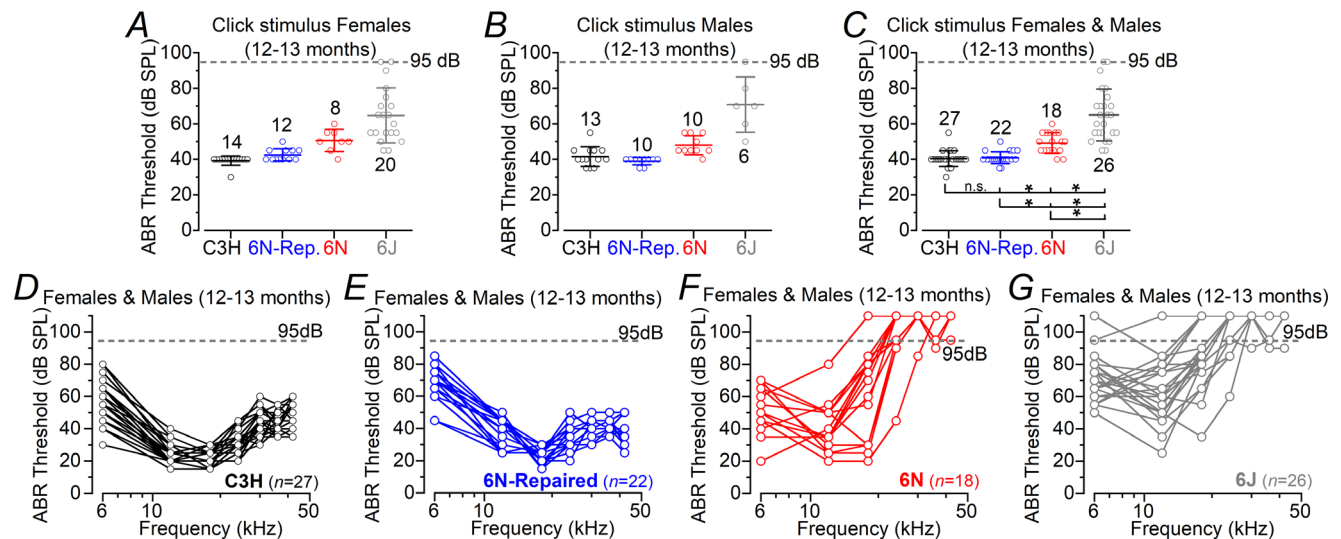

Figure 1. Auditory brainstem response thresholds in 12–13-month-old female and male mice
A and *B*, average auditory brainstem response (ABR) thresholds for clicks recorded from strain-matched aged females (*A*, 12–13 months) and males (*B*, 12–13 months) of C3H, 6N-Repaired, 6N and 6J mice. *C*, comparison of ABR thresholds for clicks when males and females in each strain were combined. A few mice included in this figure were from Jeng *et al.* (2020a): C3H: 7 out of 27; 6N-Repaired: 5 out of 22; 6N: 6 out of 18; 6J: 6 out of 26. The number of mice tested for each sex/strain is shown above or below the average data points. The statistical information shown in panel *C* is from the Tukey's *post hoc* test (one-way ANOVA) and refers to the first age point indicated (longer vertical bar) compared with the progressively older ages. Values are listed in the main text. *D–G*, ABR thresholds for frequency-specific pure-tone stimulation from 6 kHz to 42 kHz recorded from males and females C3H (*D*), 6N-Repaired (*E*), 6N (*F*) and 6J (*G*) mice. Data are shown as ABR threshold recordings from individual mice. For the Kruskal–Wallis test reported in the main text, which was aimed at comparing the ABR thresholds at 12 kHz (combined males and females: *D–G*), the Dunn's *post hoc* test values are: C3H *vs.* 6N-Repaired, $P = 0.0304$; C3H *vs.* 6N, $P = 0.0012$; C3H *vs.* 6J, $P < 0.0001$; 6N-Repaired *vs.* 6N, $P > 0.9999$; 6N-Repaired *vs.* 6J, $P < 0.0001$; 6N *vs.* 6J, $P = 0.0184$. The number of mice tested are as in panel *C*.

area. We found that, compared with 1 month, there was already a significant reduction in C_m in IHCs at 6 months of age (Fig. 2*D*: C3H: $P = 0.0074$; 6N-Repaired $P < 0.0001$; 6N: $P = 0.0002$; 6J: $P = 0.0041$, Tukey's *post hoc* test, one-way ANOVA). These results demonstrated that the IHC surface area decreased by approximately 30% from 1 to 6 months of age, independent of IHC loss. The overall reduction in IHC surface area (30–40%) was significantly different among the four strains ($P = 0.0095$, Tukey's *post hoc* test, two-way ANOVA), with C3H being different from early-onset hearing mice (6N:

$P < 0.0001$; 6J: $P = 0.0472$) but not from 6N-Repaired ($P = 0.2479$). 6N-Repaired was significantly different from 6N ($P = 0.0047$), but not from 6J mice ($P = 0.8651$), while 6N was comparable to 6J ($P = 0.0599$).

IHCs retain a normal basolateral membrane profile with age

We studied the biophysical profiles of the aged IHCs in the 9–12 kHz cochlear region of mice from both sexes
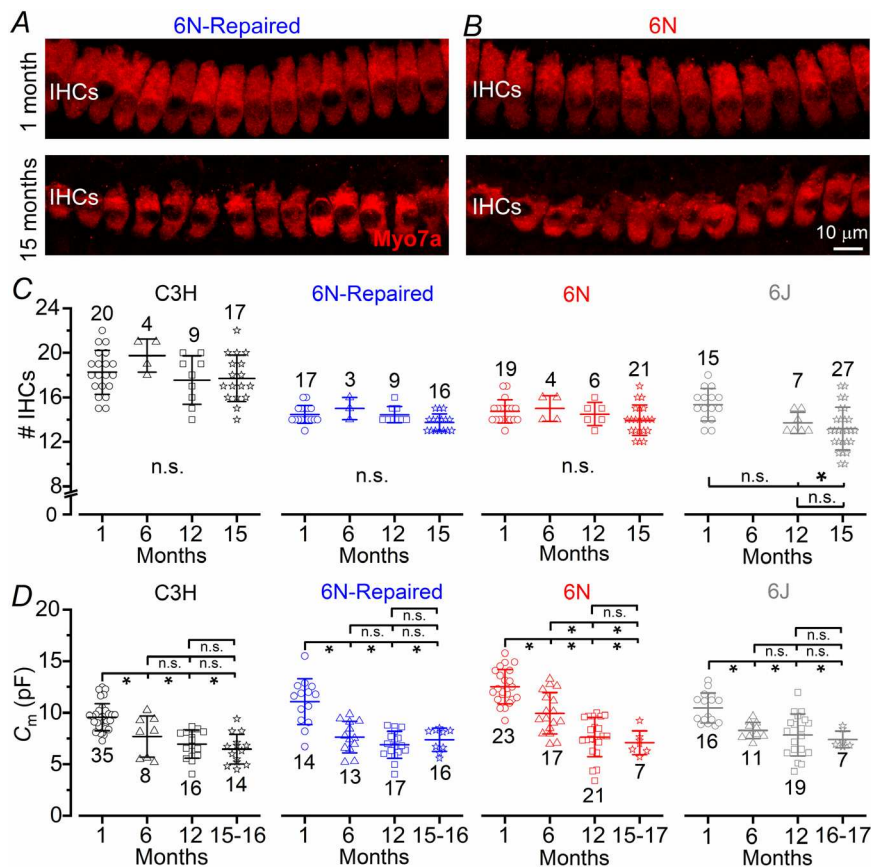

Figure 2. Inner hair cell number and size in the ageing mouse cochlea
A and *B*, maximum intensity projections of confocal z-stacks taken from the apical cochlear region (9–12 kHz) of 1-month (top panels) and 15-month-old (bottom panels) 6N-Repaired (*A*) and 6N (*B*) mice. Inner hair cells (IHCs) were labelled with an anti-myosin 7a antibody (Myo7a: red). Scale bars: 10 μm. *C*, number of IHCs present in a 140 μm region from the apical coil of 1-, 6-, 12- and 15-month-old mice. IHC counts from individual cochleae (open symbols) are plotted behind the average values. The number of cochleae investigated is shown above each set of data points. The number of IHCs decreased significantly between 1 and 15 months of age only in the 6J mice (C3H: $P = 0.9989$; 6N-Repaired: $P = 0.9884$; 6N: $P = 0.9424$; 6J: $P = 0.0016$, Tukey's *post hoc* test, one-way ANOVA). *D*, average membrane capacitance (C_m: a measure of surface area) recorded from IHCs of all four mouse strains. Single cell value recordings (open symbols) are shown behind the average values. Number of IHCs is shown below each set of data points. Number of mice from left to right: C3H 14, 5, 11, 8; 6N-Repaired 5, 3, 10, 9; 6N 12, 7, 15, 5; 6J 12, 10, 12, 5. The statistical information shown in *C* and *D* is from the Tukey's *post hoc* test (one-way ANOVA) and refers to the first age point indicated (longer vertical bar) compared with the progressively older ages. n.s. = not significant. * = in panel *C*: 6J, 1 *vs.* 15 months, $P = 0.0008$. * in panel *D*: C3H: 1 *vs.* 6 months $P = 0.0074$, 1 *vs.* 12 and 1 *vs.* 15–16 months $P < 0.0001$; 6N-Repaired: 1 *vs.* 6, 1 *vs.* 12 and 1 *vs.* 15–16 months $P < 0.0001$; 6N: 1 *vs.* 6 months $P = 0.0002$, 1 *vs.* 12 and 1 *vs.* 15–17 months $P < 0.0001$, 6 *vs.* 12 months $P = 0.0011$, 6 *vs.* 15–17 months $P = 0.0038$; 6J: 1 *vs.* 6 months $P = 0.0041$, 1 *vs.* 12 months $P < 0.0001$, 6 *vs.* 16–17 months $P = 0.0004$.

to look for further differences that might be associated with their smaller size. Mature IHCs express several K^+ channels that give rise to a large outward current (Kros *et al.* 1998; Marcotti *et al.* 2004a). One component of this K^+ current is carried by a delayed rectifier ($I_{K,s}$), which exhibits slow activation kinetics and seems to be derived from the immature K^+ current $I_{K,neo}$ (Marcotti *et al.* 2004a). The genes encoding for the Kv1.8, Kv11.1 and Kv12.1 have recently been identified to contribute to $I_{K,s}$ in IHCs (Dierich *et al.* 2020). However, the characteristic signature of fully functional mature IHCs is the expression of *Kcnma1* (Rüttiger *et al.* 2004) and *Kcnq4* (Kubisch *et al.* 1999). While *Kcnma1* encodes a BK channel carrying the rapidly activating large-conductance Ca^{2+}-activated K^+ current $I_{K,f}$ (Kros *et al.* 1998; Marcotti *et al.* 2004a), *Kcnq4* encodes a KCNQ4 channel carrying the negatively activating K^+ current $I_{K,n}$ (Marcotti *et al.* 2003; Oliver *et al.* 2003). Using a series of hyperpolarizing and depolarizing voltage steps from the holding potential of either -64 mV (Fig. 3*A* and *B*) or -84 mV (Fig. 3*C*), we found that the total K^+ current showed comparable time-course and voltage-dependence in IHCs with age across all mouse strains. Despite the smaller surface area of older IHCs (Fig. 2*D*), the size of the isolated $I_{K,n}$ remained relatively stable in all four mouse strains over the entire age range investigated (Fig. 3*D*: C3H, $P = 0.4256$; 6N-Repaired, $P = 0.1020$; 6N, $P = 0.2887$; 6J, $P = 0.0928$, one-way ANOVA over 1, 6, 12–13 and 15 months). On the other hand, $I_{K,f}$ largely decreased in size with age in IHCs from 6N and 6J mice ($P < 0.0001$; $P < 0.0001$, respectively, one-way ANOVA), less so in 6N-Repaired ($P = 0.0011$) but remained unchanged in C3H mice ($P = 0.1768$) (Fig. 3*E*). Despite the large reduction in $I_{K,f}$ in most mouse strains, the size of the total outward K^+ current (I_K) was much less affected by ageing (for statistical analysis see the legend of Fig. 3*F*). This indicated that the delayed rectifier $I_{K,s}$ is likely to be upregulated with ageing, a phenomenon also seen in some transgenic mice that fail to express the BK current in adult IHCs (e.g. Bardhan *et al.* 2019; Jeng *et al.* 2020c). While BK channels ($I_{K,f}$) are selectively located in the neck region of adult IHCs (Pyott *et al.* 2004; Jeng *et al.* 2020c), KCNQ4 channels ($I_{K,n}$) are distributed throughout the cell body (Oliver *et al.* 2003; Beisel *et al.* 2005), suggesting that the decrease in cell surface area preferentially towards their apical pole.

Voltage responses from ageing IHCs under current-clamp (Fig. 4*A*–*H*) were investigated to assess possible effects caused by the above changes in the size of the K^+ currents. Depolarizing current injection from the resting membrane potential, which to some extent mimics depolarization from the transducer current, elicited fast and graded voltage responses in IHCs from all age ranges (Fig. 4*A*–*D*). The peak voltage responses to the different current injections did not change significantly with age in all strains (C3H, $P = 0.9179$; 6N-Repaired, $P > 0.9999$; 6N,

$P = 0.7857$; 6J, $P > 0.9999$, two-way ANOVA) (Fig. 4*E*). The steady-state voltage responses changed significantly with age in 6J mice ($P = 0.0040$, two-way ANOVA) but not in the other three strains (C3H, $P = 0.9157$; 6N-Repaired, $P = 0.7106$; 6N, $P > 0.9999$) (Fig. 4*F*). To investigate the kinetics of the voltage responses, we fitted single exponentials to their onset for 100 pA current injection. The time constant of the fit became faster with age in C3H ($P = 0.0046$, one-way ANOVA) but not in the other strains (6N-Repaired, $P = 0.7901$ 6N, $P = 0.0904$; 6J, $P = 0.0615$) (Fig. 4*G*). In addition, IHCs from aged C3H mice, which showed no change in $I_{K,f}$ size (Fig. 3*E*) despite the reduction in membrane surface (Fig. 2*D*), exhibited faster voltage responses compared with those from all the other strains ($P = 0.0136$, two-way ANOVA). With age, IHCs maintained a stable *in vitro* resting membrane potential (V_m) at least up to 16–17 months of age in all strains (C3H, $P = 0.2186$; 6N-Repaired, $P = 0.1243$; 6N, $P = 0.3277$; 6J, $P = 0.8842$, one-way ANOVA, Fig. 4*H*) with no significant difference between mouse strains ($P = 0.1904$, two-way ANOVA).

Mechanoelectrical transduction is reduced in aged IHCs from mice harbouring the hypomorphic allele in Cdh23 (Cdh23^ahl)

In vivo, the basolateral membrane currents expressed in IHCs modulate the receptor potentials generated by the sound-induced opening of the MET channels. However, MET current recordings have been limited to the pre-hearing stages of development in mice because of the technical difficulties of recording from adult hair cells. In this study, we were able to perform MET recordings from IHCs of ageing mice harbouring the *Cdh23^ahl* allele (mice on the 6N background) and the 6N-Repaired strain from both sexes. Examples of MET current recordings from 1–6-, 8–10- and 14-month-old IHCs from mice carrying the *Cdh23^ahl* allele and a 9-month-old cell from the 6N-Repaired strain are shown in Fig. 5*A*–*D*. For the *Cdh23^ahl* IHCs, we have combined the data at 1 and 5–6 months as they were not significantly different ($P = 0.4027$, *t* test). We found that the maximum size of the MET current decreased significantly with age in IHCs carrying the *Cdh23^ahl* allele but not in those from the 6N-Repaired mice (Fig. 5*E*, see legend for statistical analysis). This reduction in MET current coincides with the onset of hearing loss at around the 12 kHz region in mice harbouring the *Cdh23^ahl* allele (Jeng *et al.* 2020b). Despite the different MET current size, the open probability of MET channels at rest was unaffected in both mouse strains ($P = 0.8737$, one-way ANOVA, Fig. 5*F*). These recordings indicate that age-related changes in the MET apparatus are likely to contribute to the onset and progression of hearing loss, at least in mice harbouring the
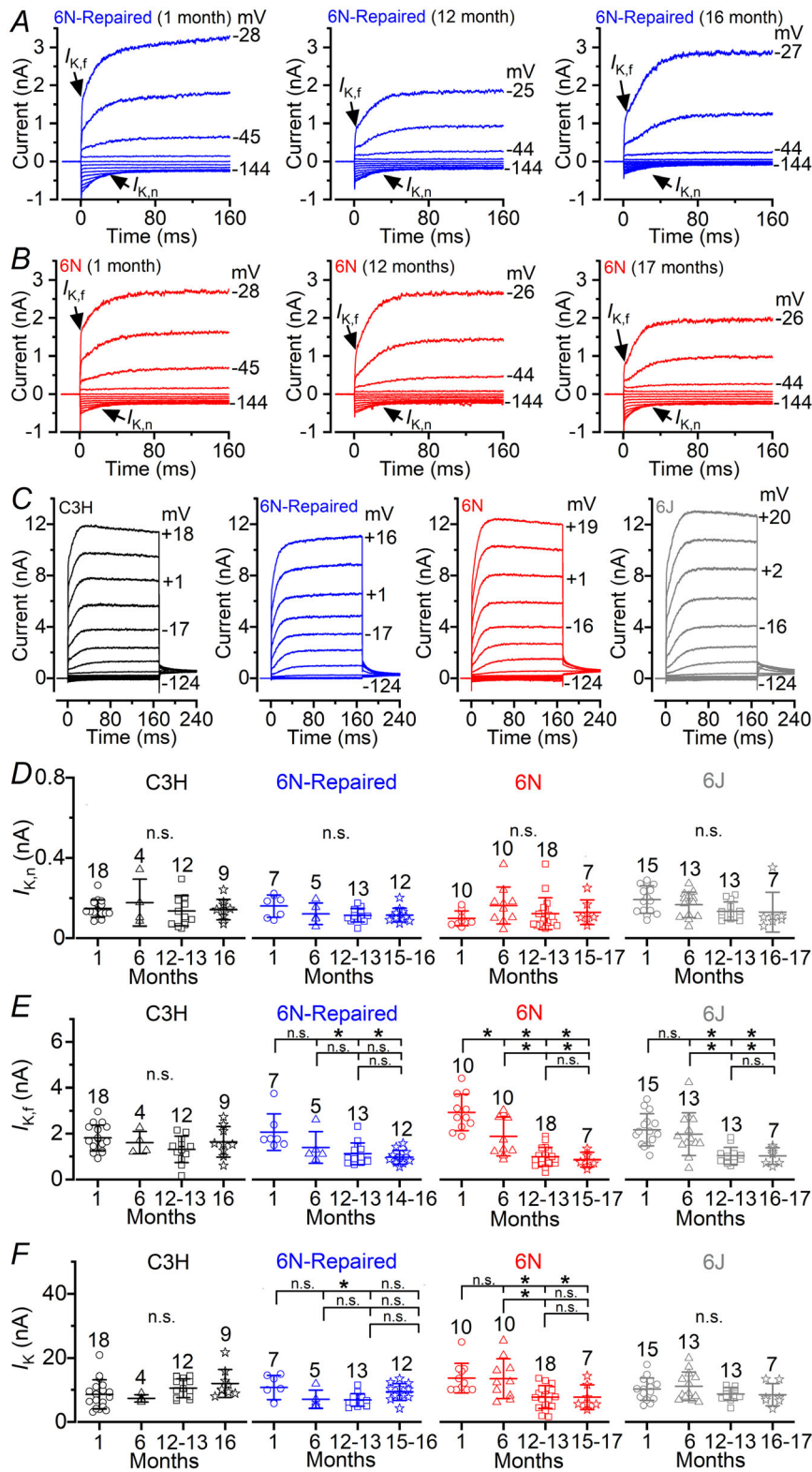
Figure 3. Potassium current recorded from inner hair cells of ageing mice

A and *B*, example of K^+ currents recorded from apical coil (9–12 kHz region) inner hair cells (IHCs) of female 6N-Repaired (*A*) and 6N (*B*) mice at 1 month (left panels), 12 months (middle panels) and 16–17 months (right panels). Currents were recorded using 10 mV depolarizing voltage steps from -144 mV (holding potential -64 mV) to the various test potentials shown by some of the traces. Holding current was plotted as zero current to facilitate the comparison between recordings. Note the presence of the deactivating $I_{K,n}$ and the fast activating $I_{K,f}$. *C*, examples of K^+ currents recorded from 12-month-old IHCs from the different strains using 10 mV depolarizing voltage steps from a holding potential -84 mV (voltage steps from -124 mV to more positive values). *D*, size of the isolated $I_{K,n}$ for the four mouse strains and at different ages, which was measured as the deactivating tail currents at -124 mV (Marcotti *et al.* 2003) from the holding potential of -84 mV. *E*, size of the isolated $I_{K,f}$ current measured at 1.5 ms from the current onset and at a membrane potential of -25 mV (Marcotti *et al.* 2003). *F*, size of the total steady-state outward K^+ current (I_K) measured at 0 mV from the holding potential of -84 mV. Single cell value recordings (open symbols) are plotted behind the average value, and were collected from both sexes. In panels *D*–*F*, the number of IHCs investigated is shown above the average data points. The statistical information shown above the data is from the Tukey's *post hoc* test (two-way ANOVA) and refers to the first age point indicated (longer vertical bar) compared with the progressively older ages. Values are listed in the Supplementary Statistical Summary.
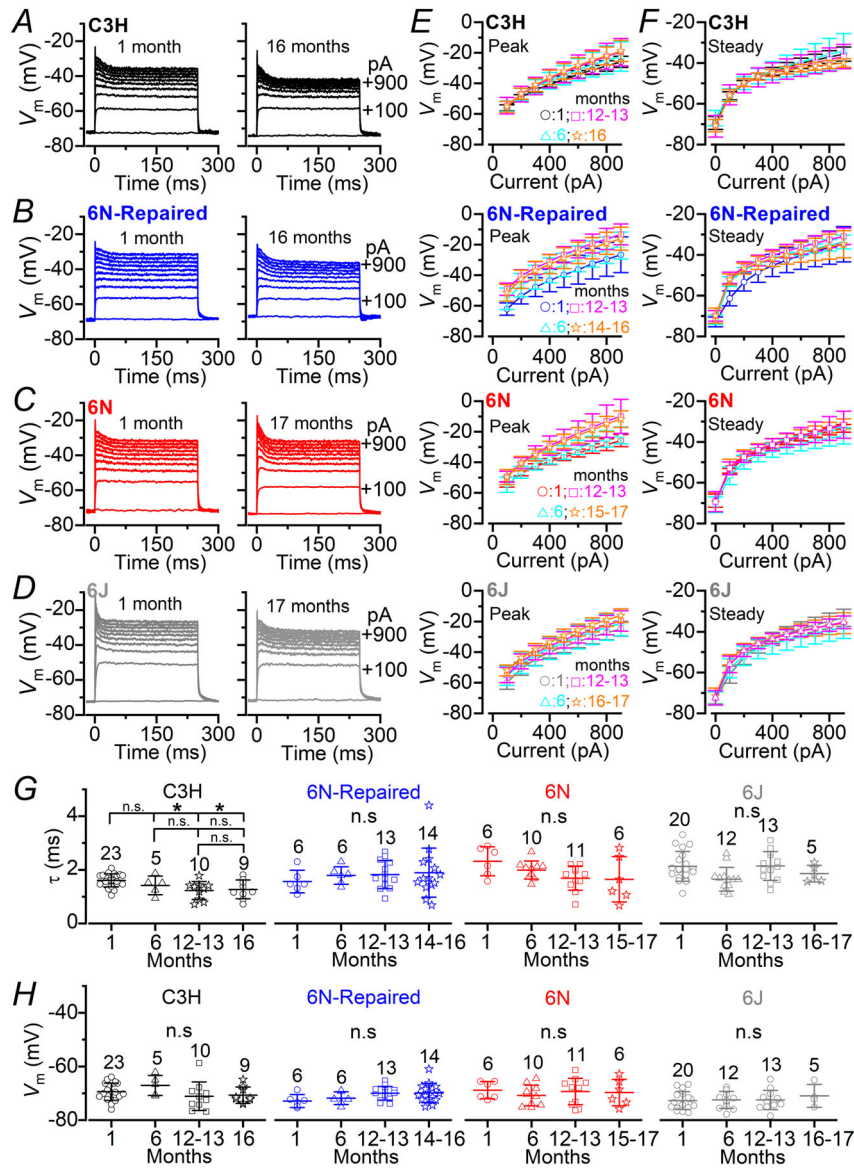
Figure 4. Ageing inner hair cells maintain near-normal voltage responses

A–D, example of voltage responses elicited by applying a series of 100 pA depolarizing current injections (up to 900 pA), from their respective membrane potentials, to 1 and either 16- or 17-month-old inner hair cells (IHCs) from the four mouse strains. *E* and *F*, relationship between the peak (*E*) and steady-state (*F*) voltage responses recorded from IHCs during the application of different current injections, as indicated in panels *A–D*. For the steady-state voltage responses obtained in 6J mice (*F*), which show significant differences with two-way ANOVA (see text), the Tukey's *post hoc* test values are: 1 *vs.* 6 months, $P < 0.0001$; 1 *vs.* 12 months, $P = 0.9212$; 1 *vs.* 16–17 months, $P < 0.0001$; 6 *vs.* 12 months, $P < 0.0001$; 6 *vs.* 16–17 months, $P < 0.0001$; 12 *vs.* 16–17 months, $P = 0.7560$. At 100 pA current injection, which was used to analyse the kinetics of the voltage responses in panel *G*, the peak V_m comparison within each strain using one-way ANOVA was: C3H, $P = 0.7060$; 6N-Repaired, $P < 0.0001$; 6N, $P = 0.0131$; 6J, $P = 0.0044$. *G*, average time constant (τ) of voltage responses in IHCs elicited with 100 pA current injection as a function of age in the different strains. For C3H, which show significant differences with one-way ANOVA (see text), the Tukey's *post hoc* test values are: 1 *vs.* 6 months, $P = 0.5884$; 1 *vs.* 12–13 months, $P = 0.0094$; 1 *vs.* 16 months, $P = 0.0314$; 6 *vs.* 12–13 months, $P = 0.6546$; 6 *vs.* 16 months, $P = 0.8054$; 12–13 *vs.* 16 months, $P = 0.9912$. For strain comparisons, which were also different from two-way ANOVA (see text), the Tukey's *post hoc* test values are: C3H *vs.* 6N-Repaired, $P = 0.0135$; C3H *vs.* 6N, $P < 0.0001$; C3H *vs.* 6J, $P < 0.0001$; 6N-Repaired *vs.* 6N, $P = 0.2660$; 6N-Repaired *vs.* 6J, $P = 0.4601$; 6N *vs.* 6J, $P = 0.9663$. *H*, Resting membrane potential (V_m) as a function of age. Single cell value recordings (open symbols) are plotted and were collected from both sexes. The number of IHCs investigated is shown above the average data points. Number of IHCs are as listed in panels *G* and *H*.

Cdh23^{ahl} allele (Johnson *et al.* 1997; Noben-Trauth *et al.* 2003).

The LOC efferent fibres reinnervate aged IHCs

We have recently shown that defects in mechanoelectrical transduction in adult IHCs leads to rewiring of the cochlear efferent system (Corns *et al.* 2018), similar to that observed in the ageing cochlea (Lauer *et al.* 2012; Zachary & Fuchs 2015). Therefore, we investigated possible differences in the progression of efferent rewiring of the ageing cochlea between the four mouse strains. Inner hair cells normally receive direct innervation from the medial olivocochlear (MOC) cholinergic efferent fibres only during the early stages of development (Liberman, 1980; Simmons *et al.* 1996). The role of the efferent input is to modulate the frequency of Ca^{2+} action potentials that occur transiently in pre-hearing IHCs (Glowatzki & Fuchs 2000), the disruption of which leads to defects in the maturation of IHC ribbon synapses (Johnson *et al.* 2013) and the normal refinement of the tonotopic maps in the maturing brainstem (Clause *et al.* 2014).

The efferent fibres release acetylcholine (ACh), which opens nicotinic $\alpha 9\alpha 10$ ACh receptors ($\alpha 9\alpha 10$nAChRs). The subsequent Ca^{2+} influx opens the small conductance Ca^{2+}-activated K^+ channels (SK2) that drive cell hyperpolarization (Glowatzki & Fuchs 2000). Soon after the onset of hearing, mouse IHCs rapidly lose their efferent innervation (Lenoir *et al.* 1980; Simmons *et al.* 1996) and downregulate their SK2 channels and nAChRs. Thus they lose the ability to respond to ACh from about P16 (Glowatzki & Fuchs 2000; Katz *et al.* 2004; Marcotti *et al.* 2004b). In the adult mammalian cochlea, the lateral olivocochlear (LOC) efferent neurons form axo-dendritic synapses with the SGNs that innervate IHCs (Maison *et al.* 2003). However, recent studies have shown that in the ~1-year-old cochlea of 6J mice the efferent system undergoes major rewiring, with the re-appearance of direct axo-somatic efferent synapses on aged IHCs (Lauer *et al.* 2012; Zachary & Fuchs 2015).

We initially used antibodies against the presynaptic efferent terminals (ChAT) and SK2 channels to see if the efferent rewiring of aged IHCs was only a characteristic of mice harbouring the *Cdh23^{ahl}* allele (6J and 6N). As expected, we found that SK2 channels
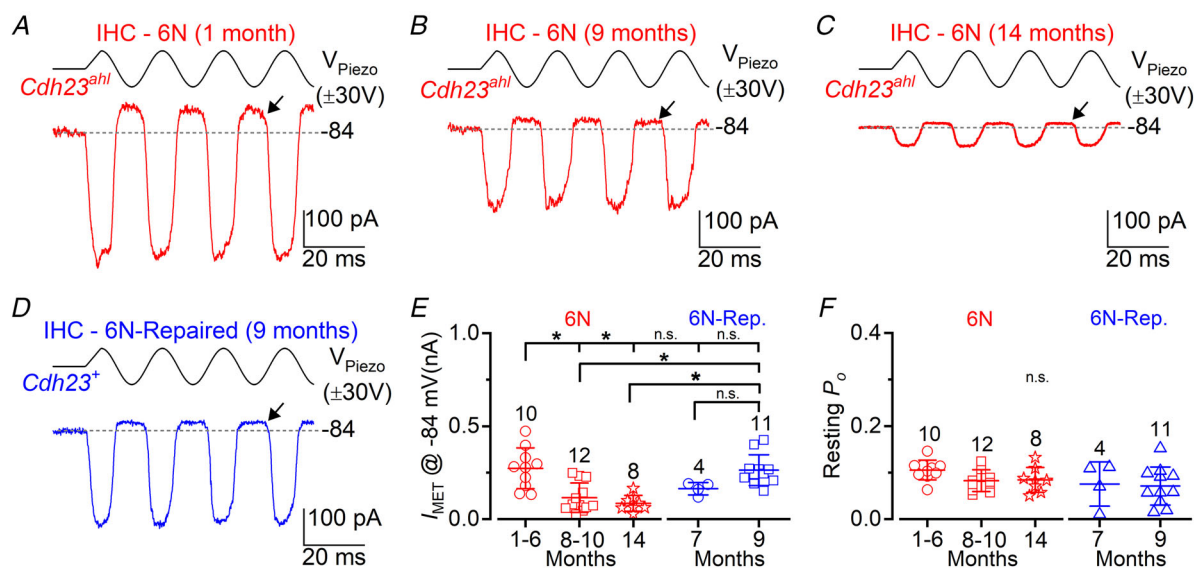

Figure 5. Mechanoelectrical transducer current is reduced in inner hair cells from ageing mice harbouring the *Cdh23^{ahl}* allele

A–D, saturating mechanoelectrical transducer (MET) currents recorded from the inner hair cells (IHCs) of 1-month (*A*), 9-month (*B*) and 14-month-old (*C*) mice harbouring the *Cdh23^{ahl}* allele (6N strain), and from a 9-month-old IHC from a 6N-Repaired mouse (*Cdh23^+*) (*D*). Recordings were done by applying sinusoidal force stimuli of 50 Hz to the hair bundles from a holding potential of -84 mV. The saturating driver voltage (V_{Piezo}) signal of ± 30 V to the fluid jet is shown above the traces (positive half-cycles of the V_{Piezo} are excitatory). The extracellular Ca^{2+} concentration was 1.3 mM. The arrows indicate complete closure of the transducer currents elicited during inhibitory bundle displacements (note that the difference in current between this level and the dashed lines represents the size of the resting MET current). Dashed lines indicate the holding current, which is the current at the holding membrane potential. *E* and *F*, maximal size (*E*) and resting open probability (*F*) of the MET current recorded from IHCs at different age ranges of 6N and 6N-Repaired mice. The number of IHCs tested is shown above the data points. The statistical information shown above the data is from the Tukey's *post hoc* test (one-way ANOVA) and refers to the first age point indicated (longer vertical bar) compared with the progressively older ages. Values are listed in the Supplementary Statistical Summary.

were absent or rarely observed in IHCs at 1 month of age (Fig. 6*A* and *B*) despite being present and juxtaposed to ChAT-immunoreactivity (efferent terminals) at P11 (Fig. 6*C*). However, in aged IHCs we observed the reappearance of juxtaposed SK2 and ChAT puncta not only in 15-month-old 6J and 6N mice (Fig. 6*D* shows an example from 6N) but also in 6N-Repaired mice (Fig. 6*E*). Only a few IHCs from C3H mice showed SK2 puncta (see below). We then quantified the percentage of ageing IHCs expressing the SK2 channels in 140 μm from the 9–12 kHz apical coil region (Fig. 6*F* and *G*). At 15 months of age, we found that the large majority of SK2 puncta were detected in the modiolar compared with the pillar side of IHCs from both late-onset (6N-Repaired and C3H, $P = 0.0004$, Tukey's *post hoc* test, one-way ANOVA) and early-onset hearing loss mice (6N/6J: $P = 0.0002$) (Fig. 6*F*). We then investigated age-related changes in the percentage of IHCs expressing SK2 channels in the four separate mouse strains, and found that it increased significantly between 1 and 15 months in 6N-Repaired, 6N and 6J mice

($P = 0.0003$, $P = 0.0131$ and $P < 0.0001$, respectively, Tukey's *post hoc* test, two-way ANOVA, Fig. 6*G*). Although the number of SK2 puncta in IHCs from aged C3H mice was not significantly different between 1 and 15 months ($P = 0.8886$), some IHCs seem to have a larger number of SK2-puncta than those in younger mice, suggesting the possibility that in these mice the efferent reinnervation might be delayed compared with the other strains. The efferent reinnervation of aged IHCs is therefore correlated with the level of hearing loss in the 12 kHz region observed in the different mouse strains at 14–18 months (Jeng *et al.* 2020b).

In order to test whether these axo-somatic (efferent-IHC) synapses in aged IHCs were functional, we perfused the cochlea with a solution containing 40 mM KCl (high K$^+$) concentration. High K$^+$ is expected to depolarize the efferent synaptic terminals and trigger the release of ACh-containing vesicles, which generates synaptic currents in IHCs superimposed upon a sustained inward current (Fig. 7*A*) induced by the superfusion of KCl on

Figure 6. Efferent synapses returning onto aged inner hair cells

A–E, maximum intensity projections of confocal z-stacks taken from the apical cochlear region of 6N (*A* and *D*) and 6N-Repaired (*B* and *E*) mice at 1 and 15 months and 6J mice (*C*) at postnatal day 11. Cochleae were labelled with antibodies against SK2 channels (green) and the efferent marker ChAT (red). Myosin 7a (Myo7a: grey) was used as an inner hair cell (IHC) marker. Scale bars: 10 μm. In each panel (*A–E*), the lower sets of three images are enlarged versions of the above images (indicated by the arrows only in panel *A*), showing the SK2 puncta juxtaposed to the ChAT-positive efferent terminals (arrowheads). Scale bars for the lower panels: 5 μm. *F*, percentage of SK2 channels that are preferentially expressed in the modiolar or pillar side of aged IHCs (15 months) from the late-onset hearing loss (C3H and 6N-Repaired) and early-onset hearing loss mice (6N and 6J). The number of mice are shown below the average modiolar data. *G*, percentage of IHCs located in the apical coil cochlear region (140 μm) showing SK2 puncta at 1, 6 and 15 months in C3H, 6N, 6N-Repaired and 6J mice. Data are plotted as mean values ± SD and individual counts are also shown (open symbols). Numbers above the data represent the number of mice (IHCs) used for each time point.
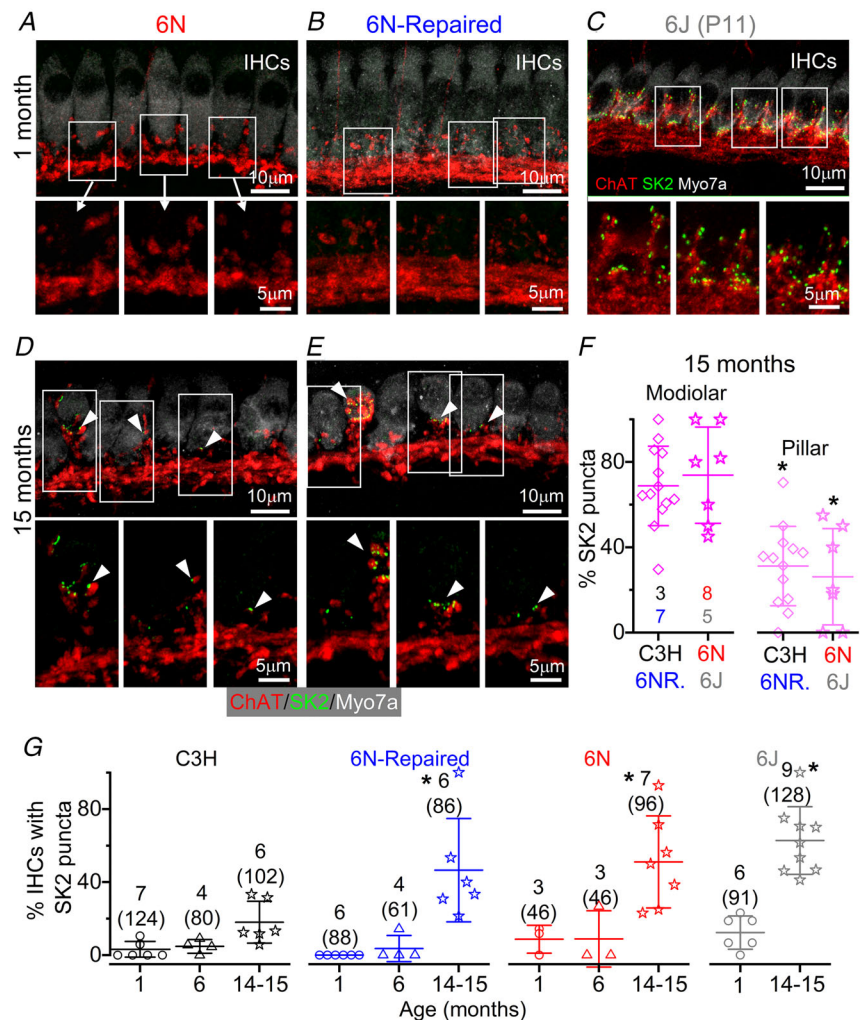
the IHC (Glowatzki & Fuchs 2000; Zachary & Fuchs 2015; Corns *et al.* 2018). We found that the percentage of 14–17-month-old IHCs from mice harbouring the *Cdh23^ahl* allele showing efferent synaptic currents (6N and 6J: 63.0%, 17 out of 27) was significantly larger compared with age-matched 6N-Repaired and C3H mice (30.8%, 8 out of 26, $P = 0.0189$, Chi-square test). The size of the post-synaptic currents was not significantly different among the mouse strains ($P = 0.5525$, one-way ANOVA, Fig. 7*B*). To confirm that the IHCs showing the inward synaptic currents (Fig. 7*A*) re-expressed functional $\alpha9\alpha10$nAChRs and SK2 channels, we tested the effect of applying ACh or 0-Ca^{2+} during a depolarizing voltage step to -24 mV from the holding of -84 mV (Marcotti *et al.* 2004b). As expected, IHCs exhibiting the synaptic currents showed an ACh-activated outward current

(Fig. 7*C*) and a current that was reduced by 0-Ca^{2+} (Fig. 7*D*). We also found aged IHCs that did not show synaptic currents or ACh-activated currents (Fig. 7*E* and *F*), but did have the current component blocked by 0-Ca^{2+} (Fig. 7*G*). The number of IHCs showing this Ca^{2+}-sensitive current was not significantly different between late-onset (6N-Repaired and C3H: 40.7%, 11 out of 27 IHCs) and the early-onset hearing loss strains (6N and 6J: 22.2%, 6 out of 27 IHCs) ($P = 0.1429$, Chi-square test). Since BK channels are insensitive to the removal of extracellular Ca^{2+} (Marcotti *et al.* 2004a), this result suggests that SK2 Ca^{2+}-activated K^+ channels are expressed in IHCs prior to the establishment of the efferent-IHC axo-somatic innervation. Indeed, immunolabelling experiments indicated the presence of SK2 puncta that were not co-localized with
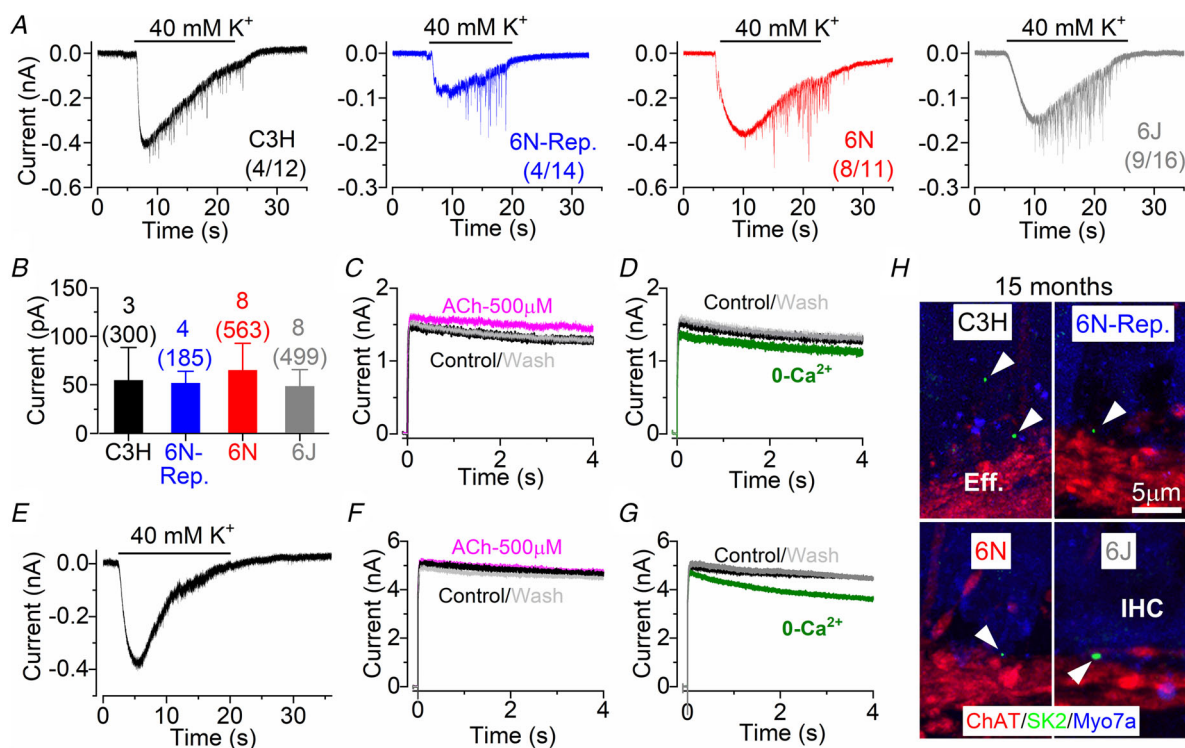

Figure 7. The axo-somatic efferent synapses on aged inner hair cells are functional
A, inward post-synaptic currents in inner hair cells (IHCs) evoked with 40 mM extracellular KCl during long-lasting recordings at -84 mV from 15-month-old C3H, 6N-Repaired, 6N and 6J mice. Numbers in brackets indicate IHCs responding to 40 mM K^+ over the total number of cells tested. *B*, average size of the inward current recorded from IHCs showing responses to 40 mM KCl. Values reported are: 54.5 ± 34.0 pA, 300 events from 3 IHCs (C3H); 51.6 ± 12.2 pA, 185 events from 4 IHCs (6N-Repaired); 64.9 ± 27.9 pA, 563 events from 8 IHCs (6N); 48.3 ± 17.3 pA, 499 events from 8 IHCs (6J). *C* and *D*, potassium currents recorded from the same IHC shown in panel *A* (6J), using a depolarizing voltage step from -84 mV to -24 mV before (Control) and after (Wash) the extracellular application of 500 μM ACh (*C*) or nominal 0-Ca^{2+} (*D*). Note that ACh increased and 0-Ca^{2+} decreased the K^+ current, which indicated the presence of $\alpha9\alpha10$nAChRs and SK2-channels, respectively, in the post-synaptic IHCs (Marcotti *et al.* 2004b). *E*–*G*, same experiments shown in panels *A*, *C* and *D*, but in this IHC (14 months, C3H mouse), 40 mM K^+ did not elicit inward post-synaptic currents (*E*). In the same IHC, while ACh did not elicit any current (*F*), 0-Ca^{2+} still decreased the K^+ current (*G*). *H*, maximum intensity projections of confocal z-stacks taken from apical IHCs of the four mouse strains at 15 months, labelled with antibodies against SK2 channels (green) and ChAT (efferent marker, red: Eff.). Myosin 7a (Myo7a: blue) was used as the IHC marker. Scale bars: 5 μm. Note SK2 channels are not juxtaposed to ChAT (arrowheads).

ChAT labelling in aged IHCs (Fig. 7*H*). These data highlight that the re-formed efferent-IHC synapses in aged mice exhibiting early-onset hearing loss are likely to be functional. Moreover, the post-synaptic SK2 channels appear prior to the establishment of the efferent contacts, suggesting that IHCs may play a direct role in re-establishing the LOC-IHC synapses.

The newly formed axo-somatic innervation between the efferent fibres and IHCs are primarily formed on the modiolar side of the cell (Fig. 6*F*), which is the region that appears most susceptible to loss of afferent synapses following noise exposure and possibly ageing (Furman *et al.* 2013; Sergeyenko *et al.* 2013). This loss of afferent synapses could effectively leave space for the rewiring of IHCs by the efferent fibres, possibly by the LOC fibres as some of them are likely to lack their normal physiological target. To test this, we performed immunostaining experiments using the anti-ATP1A3 antibody, which labels the MOC efferent neurons (McLean *et al.* 2009) known to contact the OHCs in the adult cochlea (Liberman 1980; Simmons *et al.* 1996). Since the anti-ATP1A3 antibody has also been shown to label SGNs, MOC fibres are those also showing the efferent marker ChAT. Using this approach, we confirmed that the efferent synapses onto the OHCs were MOC fibres since they showed both ATP1A3 and
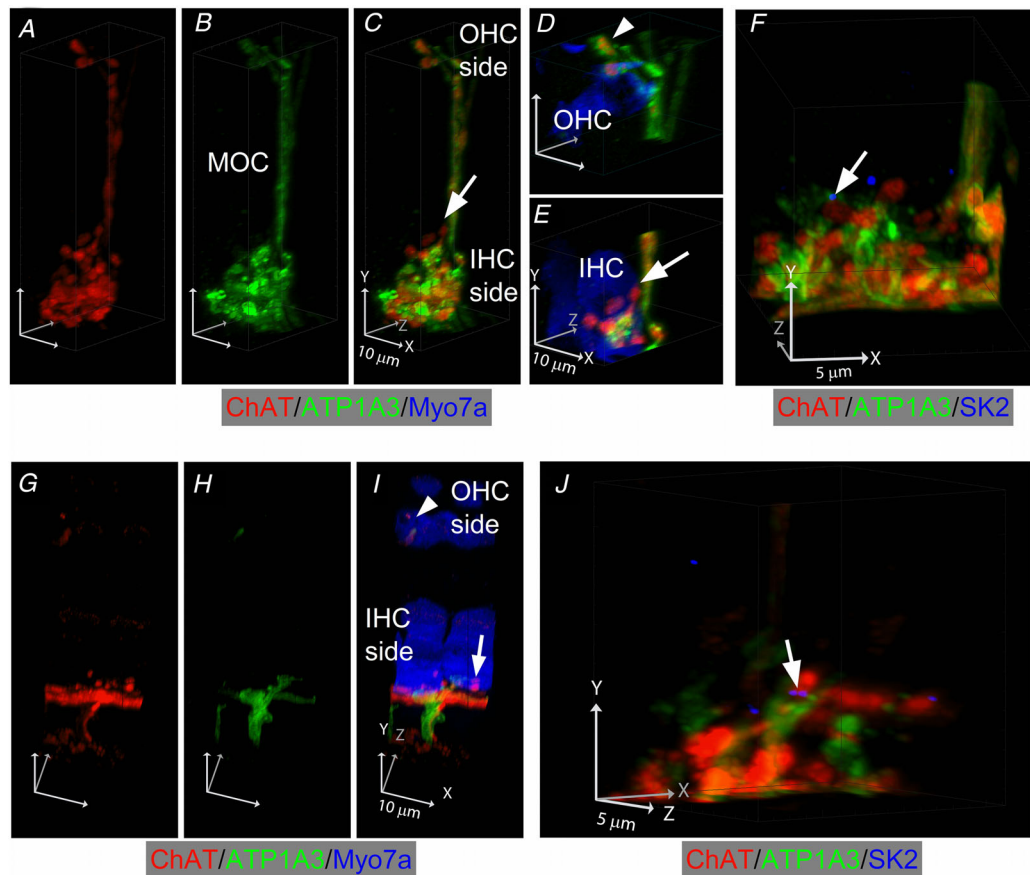

Figure 8. Lateral olivocochlear efferent terminals make axo-somatic contacts with aged inner hair cells
A–C, confocal z-stacks taken from the apical cochlea of 15-month-old C3H mice, labelled with antibodies against ChAT (*A*: red), ATP1A3 (*B*: green) and Myo7a (blue, hair cell marker). Panel *C* shows the superimposed ChAT and ATP1A3 labelling. *D* and *E*, magnified view of the outer hair cell (OHC) and inner hair cell (IHC) region from panel *C*, but also showing the hair cell marker Myo7a (blue), highlighting that the efferent terminal on OHCs are both ChAT- and ATP1A3-positive (*D*), while those contacting the IHCs are only ChAT-positive (*E*). See also Supplementary Movie. *F*, confocal z-stacks taken from the apical cochlea of aged C3H mice, labelled with anti-ChAT (red), anti-ATP1A3 (green) and anti-SK2 channel (blue) antibodies, showing that SK2 puncta are next to ChAT labelling (no ATP1A3). *G–I*, confocal z-stacks taken from the apical cochlea of 15-month-old 6J mice, labelled with antibodies against ChAT (red), ATP1A3 (green) and Myo7a (blue, hair cell marker). Panel *I* shows the superimposed ChAT and ATP1A3 labelling. Note that puncta positive for ACh, but negative for the medial olivocochlear marker ATP1A3, were present on an IHC (arrow in *I*). *J*, confocal z-stacks taken from the apical cochlea of 15-month-old 6J mice labelled with anti-ChAT (red), anti-ATP1A3 (green) and anti-SK2 channel (blue) antibodies, showing that SK2 puncta are next to ChAT labelling (no ATP1A3).

ChAT labelling (arrowheads in Fig. 8*D* and *I*). However, the efferent synapses on aged IHCs were not labelled by the ATP1A3 antibody (arrows in Fig. 8*E* and *I*; Supplementary Movie), suggesting they are not MOC terminals. We also found that in aged IHCs, ChAT-positive terminals (ATP1A3 negative) were found juxtaposed to the efferent post-synaptic SK2 channel puncta (Fig. 8*F* and *J*), further supporting the finding that the ATP1A3-negative terminals (e.g. LOC terminals) are those most likely to be the ones that contact the aged IHCs.

Discussion

We have investigated the biophysical and morphological characteristics of ageing IHCs located in the apical coil of the cochlea (9–12 kHz frequency range) from C57BL/6J (6J), C57BL/6N (6N), C57BL/6NTac^{Cdh23+} (6N-Repaired) and C3H/HeJ (C3H) mouse strains. The ABR thresholds in the 12 kHz region differed between the above four strains, with the highest thresholds recorded from 6N and 6J mice, lower thresholds from 6N-Repaired and the lowest from C3H (Fig. 9: for older ages see
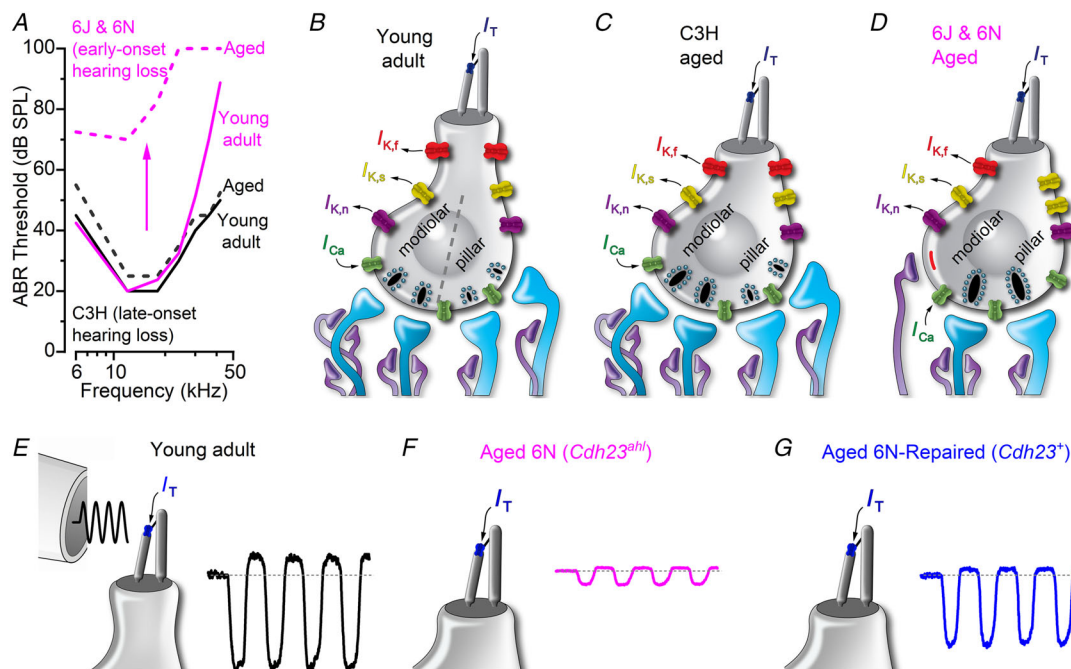

Figure 9. Schematic diagram of the biophysical and morphological changes in aged inner hair cells
A, auditory brainstem response (ABR) thresholds for frequency-specific pure-tone stimulation from 6 kHz to 42 kHz recorded from C3H (black, late-onset hearing loss) and both 6N and 6J (magenta, early-onset hearing loss) mice at 1–3 months (young adult) and 14–18 months (aged). Data are shown as average median values (solid lines) from Jeng *et al.* 2020b. Note the substantial increase in ABRs in 6J and 6N mice (arrow). *B–D*, schematic representation of the basolateral membrane protein profile and innervation pattern of IHCs from young adult (*B*) and aged C3H (*C*) and from 6J and 6N (*D*) mice. Dashed grey line in *B* indicates the separation of the IHC modiolar and pillar aspects. With age, the number of BK channels (red, carrying $I_{K,f}$) is largely reduced in early-onset hearing loss mice (*D*) but not in C3H mice (*B*). KCNQ4 channels (purple: $I_{K,n}$) are unchanged in all strains. Channels carrying $I_{K,s}$ (yellow) appear to increase only in early-onset hearing loss mice. The afferent (blue) and efferent (light purple) fibres are present at both ages, but become highly reduced in number only in aged IHCs from 6J and 6N mice (*D*). Direct axo-somatic efferent synapses, most likely of the lateral olivocochlea system (Fig. 8 and Supplementary Movie), primarily target IHCs from early-onset hearing loss mice at least up to 15 month of age. The number of ribbon synapses is largely unaffected in C3H mice, but substantial changes are present in 6J and 6N mice (see also: Jeng *et al.* 2020b). Note that the size of IHCs is reduced from 6 months of age in all strains. The decrease in IHC surface area with age is likely to occur primarily in the neck region since: (1) BK channels are specifically expressed in the neck region and their number decreases with age (Fig. 3); and (2) ribbon synapses are lost only at later stages (Jeng *et al.* 2020b). Because aged 6N-Repaired mice showed an intermediate phenotype in some of the biophysical and morphological features compared with C3H and both 6N and 6J mice, it was difficult to represent them in a diagram; they are highlighted in the Supplementary Table. *E–G*, schematic representation of the apical portion of IHCs with the mechanoelectrical transducer (MET) apparatus being stimulated by the piezo-driven fluid jet (*E*). The MET current was reduced in size with age in IHCs from mice carrying the *Cdh23^{ahl}* allele (*F*, 6N strain), but not in 6N-Repaired mice (*G, Cdh23^{+}*). Overall, C3H mice showed very little or no change associated with cochlear ageing up to at least 1.5 years of age, while 6J and 6N mice exhibited a wide range of age-related changes in their biophysical and morphological profiles. 6N-Repaired mice exhibited an intermediate hearing phenotype between C3H and both 6J and 6N strains (for ribbon synapses see: Jeng *et al.* 2020b).

Jeng *et al.* 2020b). Despite the elevated ABR thresholds present in most of the aged mouse strains, we did not observe any sign of IHC degeneration in this apical cochlea region at least up to 17 months of age. However, IHCs from all strains exhibited a progressive decrease in their surface area from earlier than 6 months of age. In most mouse strains, the smaller IHCs had a reduced BK ($I_{K,f}$) but an unaffected KCNQ4 ($I_{K,n}$) current size. These basolateral membrane changes did not alter the resting membrane potentials of IHCs (V_m: about -70 mV), since the contribution of the resting MET current is minimal *in vitro* (Johnson *et al.* 2011) and $I_{K,n}$ is the main current active at such negative V_m (Marcotti *et al.* 2003; Oliver *et al.* 2003). The reduction in IHC surface area and size of $I_{K,f}$ was most severe for 6N and 6J, less so for 6N-Repaired and minimal or absent in C3H mice (Fig. 9, Supplementary Table), which correlates with their degree of hearing loss in this cochlear region (Jeng *et al.* 2020b). We also found that direct rewiring of aged IHCs by LOC efferent neurons occurred in all strains apart from C3H mice (at least at 15 months of age, Fig. 9, Supplementary Table), but well after the onset of reduction in IHC size (Fig. 6*D*; for 6J mice see also Zachary & Fuchs, 2015). Finally, the MET current in IHCs was progressively reduced between 1–6 and 14 months of age in mice harbouring the *Cdh23^ahl* allele but not in the 6N-Repaired strain up to at least 9 months. This supports the hypothesis that hearing loss in these mice is associated with a progressive deterioration of the MET apparatus (Johnson *et al.* 1997; Noben-Trauth *et al.* 2003).

Morphological and physiological changes in IHCs with age

The surface area of IHCs located in the 9–12 kHz region was reduced by 30–40% during ageing, depending on mouse strain. Loss of cellular area or cell atrophy is a common feature of ageing, for example, in the Purkinje cells of the cerebellum (de Graaf *et al.* 2013) and neurons in the medial nucleus of the trapezoid body in the gerbil auditory brainstem (Gleich & Strutz, 2002). It is distinct from the shrinkage generally associated with apoptosis (e.g. Bortner & Cidlowski, 2003; Pini *et al.* 2016), since in IHCs it does not lead to their loss at older ages (Fig. 2). The absence of IHC loss in these four strains with ageing is consistent with previous studies in CBA/CaJ (Sergeyenko *et al.* 2013) and 6J mice (Stamataki *et al.* 2006). Reduction in cell size has been explained in terms of an adaptive response to a variety of physiological stimuli (Ginzberg *et al.* 2015; Miettinen & Björklund, 2016). Larger cells tend to have higher metabolic demands (Giordano *et al.* 1993; Ginzberg *et al.* 2015; Miettinen & Björklund, 2016). IHCs have high energy demands and numerous mitochondria (Pickles, 2004; Crawley & Keithley, 2011) and the reduction in size during ageing could potentially reduce their overall energy consumption and metabolic stress, and thus help to maintain optimal function. The loss of basolateral membrane is likely to affect primarily the upper portion of the IHCs ('neck' region) since only $I_{K,f}$ was significantly reduced in most strains, which is carried by extrasynaptic BK channels (Pyott *et al.* 2004; Jeng *et al.* 2020c). Despite the changes in size and expression of $I_{K,f}$, the *in vitro* resting membrane potentials (V_m) and voltage responses in IHCs remained largely unaffected with age. One of the unique characteristics of C3H mice was that the number of IHCs in the 9–12 kHz cochlear region was significantly larger (∼20%) than the other three strains throughout life, therefore increasing their neural sampling. C3H mice appear to be ideal for studies of late-onset ARHL because they maintain normal hearing sensitivity at least until 18 months of age across all sound frequencies (Jeng *et al.* 2020b) and their IHCs show few age-related changes.

Efferent fibre rewiring

The efferent neurons help to maintain cochlear sensitivity in noisy environments and to reduce noise-induced cochlear damage (Fuchs & Lauer, 2019). In the adult cochlea the lateral olivocochlear efferent neurons (LOC) make direct contact with type I SGNs close to where they innervate the IHCs, but with ageing they re-form functional axo-somatic synapses (6J mice: Lauer *et al.* 2012; Zachary & Fuchs, 2015). We have demonstrated that the efferent rewiring of aged IHCs occurs not only in strains carrying the *Cdh23^ahl* allele (6J and 6N), but also in 6N-Repaired mice. Interestingly, efferent axo-somatic synapses were only occasionally observed in a few IHCs from the 'good-hearing' C3H mice at 15 months of age. Thus the degree of efferent rewiring appeared to be scaled to the degree of hearing loss observed in these mice (Fig. 9). The majority of these efferent synapses were predominantly positioned on the modiolar side of IHCs. Since the SGNs innervating the modiolar side of the IHCs receive a larger number of cholinergic LOC efferent synapses than the fibres contacting the pillar side (Liberman *et al.* 1990), SGN loss induced by noise exposure or ageing (Furman *et al.* 2013; Sergeyenko *et al.* 2013) could trigger unconnected LOC terminals to form axo-somatic connections with IHCs. Indeed, we provide evidence that the LOC fibres are likely to be those innervating the aged IHCs. However, our electrophysiological and morphological experiments suggest that, at least in some IHCs, it is the post-synaptic SK2 channels that appear prior to the establishment of the efferent contact, raising the possibility that the IHCs actively attract the LOC fibres.

Impairment of the efferent cochlear innervation causes 'premature' ageing (Liberman *et al.* 2014) and an increased susceptibility to noise-induced damage (Maison *et al.* 2013). Although the role of the LOC system is less-well understood compared with that of the MOC, it is involved in inhibiting the activity of the SGN fibres and reducing glutamate-induced excitotoxicity (Ruel *et al.* 2001). Normally, IHCs are directly innervated by the efferent system only during the early stages of development (Glowatzki & Fuchs 2000), a time where they influence the maturation of the IHCs (Johnson *et al.* 2013) and the tonotopic maps in the maturing brainstem (Clause *et al.* 2014). It is possible that the reappearance of efferent terminals onto aged IHCs could be a response to physiological changes in the IHC's ability to transduce acoustic stimulation. Indeed, dysfunction in the MET current has been shown to cause the re-establishment of direct axo-somatic efferent contacts with adult IHCs (Corns *et al.* 2018). As in development, the direct efferent modulation of IHCs could influence the organization of central synapses, thus adapting to progressive changes in sound transduction. Understanding whether efferent rewiring has a positive or negative effect on the ageing cochlea is of fundamental biological importance. As we begin to think about therapeutic strategies to combat ARHL, should we be trying to prevent, or promote, the efferent rewiring of IHCs?

Mechanisms leading to the progressive elevation of ABR thresholds with age

Loss of OHCs with age is likely to play a key role in the progression of hearing loss (e.g. Kusunoki *et al.* 2004; Sergeyenko *et al.* 2013). However, this seems unlikely in the 9–12 kHz cochlear region since we observed a similar degree of OHC loss among mouse strains exhibiting very different progressive hearing loss profiles (Jeng *et al.* 2020a). Here, we have shown that in addition to the decrease in IHC surface area with age, the size of the BK current $I_{K,f}$ decreased and the delayed rectifier $I_{K,s}$ is likely to increase, with age in all strains apart from C3H mice (Fig. 9, Supplementary Table). These morphological and physiological changes seem to allow aged IHCs to generate, at least in principle, reliable receptor potentials during *in vivo* sound stimulation. This functional compensation in ageing IHCs is also manifested in the normal size and Ca^{2+}-dependence of exocytosis in IHCs from old mice (Jeng *et al.* 2020b), despite the significant loss of ribbon synapses (Stamataki *et al.* 2006; Jeng *et al.* 2020b). Although several of these age-related changes in the IHC basolateral membrane characteristics are correlated with the level of hearing loss in the different mouse strains (Fig. 9), they are unlikely to be the only cause of the wide range of hearing sensitivity that we observed between strains (Fig. 1; see also Jeng *et al.* 2020b).

An additional contributing factor to the different hearing phenotypes is likely to be the re-establishment of axo-somatic connections with aged IHCs, which was initially demonstrated in 6J mice (Lauer *et al.* 2012; Zachary & Fuchs, 2015). These newly formed efferent LOC-IHC contacts were, like the age-related changes at ribbon synapses (Jeng *et al.* 2020b), correlated with the degree of hearing loss in the different mouse strains. They are mainly associated with mice showing some degree of hearing loss within the 12 kHz cochlear region (6J, 6N and 6N-Repaired) and they are minimal in the good-hearing C3H mice (efferent: Fig. 9, see also Supplementary Table; ribbon synapses see: Jeng *et al.* 2020b). We also found that the MET current in IHCs from mice harbouring the $Cdh23^{ahl}$ allele became smaller with age, which was not evident in the isogenic 6N-Repaired mice. Similar MET reduction was found in ageing OHCs from mice harbouring the $Cdh23^{ahl}$ allele (Jeng *et al.* 2020a), suggesting that age-related changes in the MET apparatus might play an important role in the differential progression of ARHL. This finding complements previous reports showing that the normal morphology of the stereociliary bundle is progressively altered with age (Bohne *et al.* 1990; Bullen *et al.* 2019) and that the $Cdh23^{ahl}$ allele is responsible for the early-onset hearing loss in 6J and 6N mice (Johnson *et al.* 1997; Noben-Trauth *et al.* 2003).

The results presented in this study, together with those showing the progression of age-related changes in IHC ribbon synapses (Jeng *et al.* 2020b) and in the OHCs and their innervation pattern (Jeng *et al.* 2020a), indicate that multiple processes with various time courses in the ageing mouse cochlea accumulate over time and contribute to the progression of ARHL.

References

Bardhan T, Jeng JY, Waldmann M, Ceriani F, Johnson SL, Olt J, Rüttiger L, Marcotti W & Holley MC (2019). Gata3 is required for the functional maturation of inner hair cells and their innervation in the mouse cochlea. *J Physiol* **597**, 3389–3406.

Beisel KW, Rocha-Sanchez SM, Morris KA, Nie L, Feng F, Kachar B, Yamoah EN & Fritzsch B (2005). Differential expression of KCNQ4 in inner hair cells and sensory neurons is the basis of progressive high-frequency hearing loss. *J Neurosci* **25**, 9285–9293.

Beurg M, Fettiplace R, Nam JH & Ricci AJ (2009). Localization of inner hair cell mechanotransducer channels using high-speed calcium imaging. *Nat Neurosci* **12**, 553–558.

Bohne BA, Gruner MM & Harding GW (1990). Morphological correlates of aging in the chinchilla cochlea. *Hear Res* **48**, 79-91.

Bortner CD & Cidlowski JA (2003). Uncoupling cell shrinkage from apoptosis reveals that Na+ influx is required for volume loss during programmed cell death. *J Biol Chem* **278**, 39176–39184.

Bowl MR & Dawson SJ (2019). Age-related hearing loss. *Cold Spring Harb Perspect Med* **9**, a033217.

Bullen A, Forge A, Wright A, Richardson GP, Goodyear RJ & Taylor R (2019). Ultrastructural defects in stereocilia and tectorial membrane in aging mouse and human cochleae. *J Neurosci Res* **98**, 1745-1763.

Ceriani F, Hendry A, Jeng JY, Johnson SL, Stephani F, Olt J, Holley MC, Mammano F, Engel J, Kros CJ, Simmons DD & Marcotti W (2019). Coordinated calcium signalling in cochlear sensory and non-sensory cells refines afferent innervation of outer hair cells. *EMBO J* **38**, pii: e99839.

Clause A, Kim G, Sonntag M, Weisz CJ, Vetter DE, Rűbsamen R & Kandler K (2014). The precise temporal pattern of prehearing spontaneous activity is necessary for tonotopic map refinement. *Neuron* **82**, 822–835.

Corns LF, Johnson SL, Kros CJ & Marcotti W (2014). Calcium entry into stereocilia drives adaptation of the mechano-electrical transducer current of mammalian cochlear hair cells. *Proc Natl Acad Sci USA* **111**, 14918–14923.

Corns LF, Johnson SL, Roberts T, Ranatunga KM, Hendry A, Ceriani F, Safieddine S, Steel KP, Forge A, Petit C, Furness DN, Kros CJ & Marcotti W (2018). Mechanotransduction is required for establishing and maintaining mature inner hair cells and regulating efferent innervation. *Nature Comm* **9**, 4015.

Crawley BK & Keithley EM (2011). Effects of mitochondrial mutations on hearing and cochlear pathology with age. *Hear Res* **280**, 201–208.

de Graaf EL, Vermeij WP, de Waard MC, Rijksen Y, van der Pluijm I, Hoogenraad CC, Hoeijmakers JH, Altelaar AF & Heck AJ (2013). Spatio-temporal analysis of molecular determinants of neuronal degeneration in the aging mouse cerebellum. *Mol Cell Proteomics* **12**, 1350–1362.

Dierich M, Altoè A, Koppelmann J, Evers S, Renigunta V, Schäfer MK, Naumann R, Verhulst S, Oliver D & Leitner MG (2020). Optimized tuning of auditory inner hair cells to encode complex sound through synergistic activity of six independent K+ current entities. *Cell Rep* **32**, 107869.

Fuchs PA & Lauer AM (2019). Efferent inhibition of the cochlea. *Cold Spring Harb Perspect Med* **9**, a033530.

Furman AC, Kujawa SG & Liberman MC (2013). Noise-induced cochlear neuropathy is selective for fibers with low spontaneous rates. *J Neurophysiol* **110**, 577–586.

Giordano E, Cirulli V, Bosco D, Rouiller D, Halban P & Meda P (1993). B-cell size influences glucose-stimulated insulin secretion. *Am J Physiol* **265**, C358–C364.

Ginzberg MB, Kafri R & Kirschner M (2015). Cell biology. On being the right (cell) size. *Science* **348**, 1245075.

Gleich O & Strutz J (2002). Age dependent changes in the medial nucleus of the trapezoid body in gerbils. *Hear Res* **164**, 166–178.

Glowatzki E & Fuchs PA (2000). Cholinergic synaptic inhibition of inner hair cells in the neonatal mammalian cochlea. *Science* **288**, 2366–2368.

Guimaraes P, Zhu X, Cannon T, Kim S & Frisina RD (2004). Sex differences in distortion product otoacoustic emissions as a function of age in CBA mice. *Hear Res* **192**, 83–89.

Henry KR (2004). Males lose hearing earlier in mouse models of late-onset age-related hearing loss; females lose hearing earlier in mouse models of early-onset hearing loss. *Hear Res* **190**, 141-148.

Hequembourg S & Liberman MC (2001). Spiral ligament pathology: a major aspect of age-related cochlear degeneration in C57BL/6 mice. *J Assoc Res Otolaryngol* **2**, 118–129.

Kane KL, Longo-Guess CM, Gagnon LH, Ding D, Salvi RJ & Johnson KR (2012). Genetic background effects on age-related hearing loss associated with Cdh23 variants in mice. *Hear Res* **283**, 80–88.

Katz E, Elgoyhen AB, Gomez-Casati ME, Knipper M, Vetter DE, Fuchs PA & Glowatzki E (2004). Developmental regulation of nicotinic synapses on cochlear inner hair cells. *J Neurosci* **24**, 7814–7820.

Kazmierczak P, Sakaguchi H, Tokita J, Wilson-Kubalek EM, Milligan RA, Muller U & Kachar B (2007). Cadherin 23 and protocadherin 15 interact to form tip-link filaments in sensory hair cells. *Nature* **449**, 87–91.

Kobrina A & Dent ML (2019). The effects of age and sex on the detection of pure tones by adult CBA/CaJ mice (*Mus musculus*). *J Neurosci Res* **15**, 10.

Kros CJ, Ruppersberg JP & Rüsch A (1998). Expression of a potassium current in inner hair cells during development of hearing in mice. *Nature* **394**, 281–284.

Kubisch C, Schroeder BC, Friedrich T, Lütjohann B, El-Amraoui A, Marlin S, Petit C & Jentsch TJ (1999). KCNQ4, a novel potassium channel expressed in sensory outer hair cells, is mutated in dominant deafness. *Cell* **96**, 437–446.

Kusunoki T, Cureoglu S, Schachern PA, Baba K, Kariya S & Paparella MM (2004). Age-related histopathologic changes in the human cochlea: a temporal bone study. *Otolaryngol Head Neck Surg* **131**, 897–903.

Ingham NJ, Pearson S & Steel KP (2011). Using the auditory brainstem response (ABR) to determine sensitivity of hearing in mutant mice. *Curr Protoc Mouse Biol* **1**, 279–287.

Jeng JY, Johnson SL, Carlton AJ, De Tomasi L, Goodyear RJ, De Faveri F, Furness DN, Wells S, Brown SDM, Holley MC, Richardson GP, Mustapha M, Bowl MR & Marcotti W (2020*a*). Age-related changes in the biophysical and morphological characteristics of mouse cochlear outer hair cells. *J Physiol* **598**, 3891-3910.

Jeng JY, Ceriani F, Olt J, Brown SDM, Holley MC, Bowl MR, Johnson SL & Marcotti W (2020*b*). Pathophysiological changes in inner hair cell ribbon synapses in the ageing mammalian cochlea. *J Physiol* **598**, 4339-4355.

Jeng JY, Ceriani F, Hendry A, Johnson SL, Yen P, Simmons DD, Kros CJ & Marcotti W (2020*c*) Hair cell maturation is differentially regulated along the tonotopic axis of the mammalian cochlea. *J Physiol* **598**, 151–170.

Jimenez JE, Nourbakhsh A, Colbert B, Mittal R, Yan D, Green CL, Nisenbaum E, Liu G, Bencie N, Rudman J, Blanton SH & Zhong Liu X (2020). Diagnostic and therapeutic applications of genomic medicine in progressive, late-onset, nonsyndromic sensorineural hearing loss. *Gene* **747**, 144677

Johnsson LG (1974). Sequence of degeneration of Corti's organ and its first-order neurons. *Ann Otol Rhinol Laryngol* **83**, 294.

Johnson KR, Erway LC, Cook SA, Willott JF & Zheng QY (1997). A major gene affecting age-related hearing loss in C57BL/6J mice. *Hear Res* **114**, 83–92.

Johnson SL, Beurg M, Marcotti W & Fettiplace R (2011). Prestin-driven cochlear amplification is not limited by the outer hair cell membrane time constant. *Neuron* **70**, 1143–1154.

Johnson SL, Wedemeyer C, Vetter DE, Adachi R, Holley MC, Elgoyhen AB & Marcotti W (2013). Cholinergic efferent synaptic transmission regulates the maturation of auditory hair cell ribbon synapses. *Open Biol* **3**, 130163.

Johnson SL, Safieddine S, Mustapha M & Marcotti W (2019). Hair cell afferent synapses: Function and dysfunction. *Cold Spring Harb Perspect Med* **9**, a033175.

Lauer AM, Fuchs PA, Ryugo DK & Francis HW (2012). Efferent synapses return to inner hair cells in the aging cochlea. *Neurobiol Aging* **33**, 2892–2902.

Lenoir M, Shnerson A & Pujol R (1980). Cochlear receptor development in the rat with emphasis on synaptogenesis. *Anat Embryol* **160**, 253–262.

Liberman MC (1980). Efferent synapses in the inner hair cell area of the cat cochlea: an electron microscopic study of serial sections. *Hear Res* **3**, 189–204.

Liberman MC, Liberman LD & Maison SF (2014). Efferent feedback slows cochlear aging. *J Neurosci*. **34**, 4599–4607.

Liberman MC, Dodds LW & Pierce S (1990). Afferent and efferent innervation of the cat cochlea: quantitative analysis with light and electron microscopy. *J Comp Neurol* **301**, 443–460.

Maison SF, Adams JC & Liberman MC (2003). Olivocochlear innervation in the mouse: immunocytochemical maps, crossed versus uncrossed contributions and transmitter colocalization. *J Comp Neurol* **455**, 406–416.

Maison SF, Usubuchi H & Liberman MC (2013). Efferent feedback minimizes cochlear neuropathy from moderate noise exposure. *J Neurosci* **33**, 5542–5552.

Marcotti W (2012). Functional assembly of mammalian cochlear hair cells. *Exp Physiol* **97**, 438–451.

Marcotti W, Johnson SL, Holley MC & Kros CJ (2003). Developmental changes in the expression of potassium currents of embryonic, neonatal and mature mouse inner hair cells. *J Physiol* **548**, 383–400.

Marcotti W, Johnson SL & Kros CJ (2004*a*). Effects of intracellular stores and extracellular Ca^{2+} on Ca^{2+}-activated K^{+} currents in mature mouse inner hair cells. *J Physiol* **557**, 613-633.

Marcotti W, Johnson SL & Kros CJ (2004*b*). A transiently expressed SK current sustains and modulates action potential activity in immature mouse inner hair cells. *J Physiol* **560**, 691–708.

McLean WJ, Smith KA, Glowatzki E & Pyott SJ (2009). Distribution of the Na,K-ATPase alpha subunit in the rat spiral ganglion and organ of Corti. *J Assoc Res Otolaryngol* **10**, 37–49.

Meyer AC, Frank T, Khimich D, Hoch G, Riedel D, Chapochnikov NM, Yarin YM, Harke B, Hell SW, Egner A & Moser T (2009). Tuning of synapse number, structure and function in the cochlea. *Nat Neurosci* **12**, 444–453.

Mianné J, Chessum L, Kumar S, Aguilar C, Codner G, Hutchison M, Parker A, Mallon AM, Wells S, Simon MM, Teboul L, Brown SD & Bowl MR (2016). Correction of the auditory phenotype in C57BL/6N mice via CRISPR/Cas9-mediated homology directed repair. *Genome Med* **8**, 16.

Miettinen TP & Björklund M (2016). Cellular allometry of mitochondrial functionality establishes the optimal cell size. *Dev Cell* **39**, 370–382.

Müller M, von Hünerbein K, Hoidis S & Smolders JW (2005). A physiological place-frequency map of the cochlea in the CBA/J mouse. *Hear Res* **202**, 63–73.

Noben-Trauth K, Zheng QY & Johnson KR (2003). Association of cadherin 23 with polygenic inheritance andgenetic modification of sensorineural hearing loss. *Nat Genet* **35**, 21–23.

Ohlemiller KK, Jones SM & Johnson KR (2016). Application of mouse models to research in hearing and balance. *J Assoc Res Otolaryngol* **17**, 493–523.

Oliver D, Knipper M, Derst C & Fakler B (2003). Resting potential and submembrane calcium concentration of inner hair cells in the isolated mouse cochlea are set by KCNQ-type potassium channels. *J Neurosci* **23**, 2141–2149.

Pickles JO (2004). Mutation in mitochondrial DNA as a cause of presbyacusis. *Audiol Neurootol* **9**, 23–33.

Pini L, Pievani M, Bocchetta M, Altomare D, Bosco P, Cavedo E, Galluzzi S, Marizzoni M & Frisoni GB (2016). Brain atrophy in Alzheimer's Disease and aging. *Ageing Res Rev* **30**, 25–48.

Pujol R, Lavigne-Rebillard M & Lenoir M (1998). Development of sensory and neural structures in the mammalian cochlea. In *Development of the Auditory System*, eds. Rubel EW, Popper AN & Fay RR, pp. 146–192. Springer, New York.

Pyott SJ, Glowatzki E, Trimmer JS & Aldrich RW (2004). Extrasynaptic localization of inactivating calcium-activated potassium channels in mouse inner hair cells. *J Neurosci* **24**, 9469–9474.

Ruel J, Nouvian R, Gervais d'Aldin C, Pujol R, Eybalin M & Puel JL (2001). Dopamine inhibition of auditory nerve activity in the adult mammalian cochlea. *Eur J Neurosci* **14**, 977–986.

Rüttiger L, Sausbier M, Zimmermann U, Winter H, Braig C, Engel J, Knirsch M, Arntz C, Langer P, Hirt B, Müller M, Köpschall I, Pfister M, Münkner S, Rohbock K, Pfaff I, Rüsch A, Ruth P & Knipper M (2004). Deletion of the Ca2+-activated potassium (BK) alpha-subunit but not the BKbeta1-subunit leads to progressive hearing loss. *Proc Natl Acad Sci USA* **101**, 12922–12927.

Schuknecht HF & Gacek MR (1993). Cochlear pathology in presbycusis. *Ann Otol Rhinol Laryngol* **102**, 1–16.

Sergeyenko Y, Lall K, Liberman MC & Kujawa SG (2013). Age-related cochlear synaptopathy: an early-onset contributor to auditory functional decline. *J Neurosci* **33**, 13686–13694.

Simmons DD, Mansdorf NB & Kim JH (1996). Olivocochlear innervation of inner and outer hair cells during postnatal maturation: evidence for a waiting period. *J Comp Neurol* **370**, 551–562.

Stamataki S, Francis HW, Lehar M, May BJ & Ryugo DK (2006). Synaptic alterations at inner hair cells precede spiral ganglion cell loss in aging C57BL/6J mice. *Hear Res* **221**, 104–118.

Tawfik KO, Klepper K, Saliba J & Friedman RA (2019). Advances in understanding of presbycusis. *J Neurosci Res* **98**, 1685-1697.

Trune DR, Kempton JB & Mitchell C (1996). Auditory function in the C3H/HeJ and C3H/HeSnJ mouse strains. *Hear Res* **96**, 41–45.

Wu PZ, Liberman LD, Bennett K, de Gruttola V, O'Malley JT & Liberman MC (2019). Primary neural degeneration in the human cochlea: evidence for hidden hearing loss in the aging ear. *Neurosci* **407**, 8–20.

Zachary SP & Fuchs PA (2015). Re-emergent inhibition of cochlear inner hair cells in a mouse model of hearing loss. *J Neurosci* **35**, 9701–9706.

Zampini V, Johnson SL, Franz C, Knipper M, Holley MC, Magistretti J, Masetto S & Marcotti W (2013). Burst activity and ultrafast activation kinetics of CaV1.3 Ca^{2+} channels support presynaptic activity in adult gerbil hair cell ribbon synapses. *J Physiol* **591**, 3811–3820.

Additional information

Data availability statement

The data that support the findings of this study are available from the corresponding author upon reasonable request.

Competing interests

The authors declare no conflicts of interest.

Author contributions

J-Y.J., A.J.C, S.L.J., M.C.H. and W.M. were involved in the acquisition, analysis or interpretation of data for the work. S.D.M.B. and M.R.B. were involved in the initial design and interpretation of data. All authors were involved in revising it critically for important intellectual content. J-Y.J. and W.M. conceived and designed the study and drafted the paper.

All authors approved the final version of the paper. All authors agree to be accountable for all aspects of the work in ensuring that questions related to the accuracy or integrity of any part of the work are appropriately investigated and resolved. All persons designated as authors qualify for authorship, and all those who qualify for authorship are listed.

Supporting information

Additional supporting information may be found online in the Supporting Information section at the end of the article.

Statistical Summary Document
Supplementary Movie
Supplementary Table & Movie legend